Insights into the micro-modification mechanism, thermal stability, and rheological property of SBS/TB rubber crumb modified asphalt binder

Huang, Shan; Chen, Huikun; Niu, Dongyu; Ren, Shisong; Liu, Xueyan

DOI
10.1016/j.conbuildmat.2025.141670

Publication date
2025

Document Version
Final published version

Published in
Construction and Building Materials

Construction and Building Materials 482 (2025) 141670

Contents lists available at ScienceDirect

Construction and Building Materials

journal homepage: www.elsevier.com/locate/conbuildmat

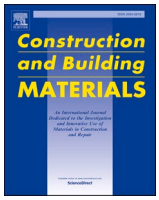

Insights into the micro-modification mechanism, thermal stability, and rheological property of SBS/TB rubber crumb modified asphalt binder

Shan Huang [a], Huikun Chen [a], Dongyu Niu [a,*], Shisong Ren [b], Xueyan Liu [c]

[a] School of Materials Science and Engineering, Chang'an University, Xi'an 710061, China
[b] Sustainable Pavement and Asphalt Research group, University of Antwerp, Antwerp 2020, Belgium
[c] School of Pavement Engineering, Faculty of Civil Engineering and Geosciences, Delft University of Technology, Stevinweg 1, Delft 2628 CN, the Netherlands

ARTICLE INFO

Keywords:
Terminal blend (TB) crumb rubber
SBS
Thermal stability
Thermal pyrolysis kinetics
Rheological property

ABSTRACT

To increase the utilization of used tires, reduce carbon emissions and improve asphalt pavement performance, SBS/TB crumb rubber modified asphalt binder was designed, which was enhanced by SBS and terminal blend (TB) crumb rubber. SBS/TB crumb rubber modified asphalt binder was prepared by mixing 0 %, 10 %, and 15 % TB crumb rubber with 2 % and 3 % SBS, respectively. This study investigated the microstructure, thermal stability and rheological properties of SBS/TB crumb rubber modified asphalt binder. The Spearman correlation coefficient is introduced to analyze the correlation of microstructural, thermodynamic and rheological parameters. The results showed that SBS and TB crumb rubber were uniformly dispersed in asphalt binder without agglomeration phenomenon. In addition, the interaction between SBS and TB crumb rubber resulted in the formation of cross-links between the polymer and the asphalt binder, significantly improving the storage stability and the thermal stability of the modified asphalt binder. The pyrolysis mechanism of the modified asphalt binder is One-dimension diffusion or One-dimension phase boundary. With the addition of SBS and TB crumb rubber, the rheological, high-and-low temperature properties of modified asphalt binder are improved. Finally, microstructural, thermodynamic and rheological parameters have an extremely strong correlation by Spearman correlation coefficient analysis.

1. Introduction

Currently, the world produces one billion waste tires each year, which are usually disposed of in landfills or incinerated, methods that have a significant negative impact on the environment and public health [1,2]. Scholars [3] have proposed recycling waste tires, and in recent years, converting waste tires into crumb rubber modifiers for use in asphalt pavements has emerged as a sustainable solution. However, the low heat resistance of crumb rubber (CR) modified asphalt binder may compromise its long-term durability. The production of waste tires in China is shown in Fig. 1.

In order to increase the utilization of waste tires, reduce the negative impact on the environment and public health, and improve the road performance of asphalt binder, many scholars [4–9] are trying to blend SBS and CR for asphalt binder modification. The research shows that SBS/CR modified asphalt binder exhibits excellent performance in terms of viscoelasticity and high-and-low temperature performance. However, SBS/CR modified asphalt binder prepared by conventional treatments required to be used in a shorter period of time due to its serious segregation and poor storage stability issues [10].

To this end, the terminal blend (TB) technology for crumb rubber was developed through fully dispersing crumb rubber particles in the asphalt binder [10–13]. Some existing studies have begun to focus on SBS/TB crumb rubber modified asphalt binder, for example, Qian [13] focused on the storage stability of SBS/TB crumb rubber modified asphalt binder, and found that TB binders with various SBS contents showed good storage stability. Wang [14] added SBS into TB crumb rubber modified asphalt binder and analyzed its anti-aging performance, and found that SBS/TB crumb rubber modified asphalt binder with 3 wt % SBS and 5 wt% TB crumb rubber, 3 wt% SBS and 20 wt% TB crumb rubber have the best short-term aging resistance and the best long-term aging resistance, respectively.Zhang and Huang [15] studied that adding 2 % SBS can improve the high-temperature performance of TB crumb rubber modified asphalt binder mixture without affecting its low-temperature performance, but adding more SBS does not bring more additional value. Huang [16] found that the fatigue life of SBS/TB

* Corresponding author.
E-mail address: niudongyu_1984@chd.edu.cn (D. Niu).

https://doi.org/10.1016/j.conbuildmat.2025.141670
Received 17 May 2024; Received in revised form 28 September 2024; Accepted 5 May 2025
Available online 9 May 2025

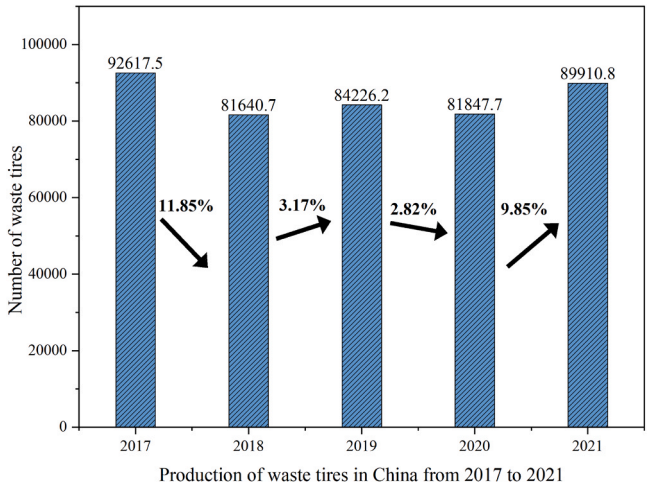

Fig. 1. Production of waste tires in China from 2017 to 2021 [4].

crumb rubber modified asphalt binder mix is twice as long as that of SBS modified asphalt binder, and its self-repair ability is better than that of ordinary SBS modified asphalt binder. It can be seen that SBS/TB crumb rubber modified asphalt binder also has good road performance. At present, although it has been known that SBS/TB crumb rubber modified asphalt binder has better high-and-low temperature performance, storage stability, rutting resistance and durability, but has not yet seen the SBS/TB crumb rubber modified asphalt binder viscoelasticity, microscopic modification mechanism of the relevant research.

Thermal stability of asphalt binder in pavement use is a key factor in the durability of its performance and the service life of the roadway. And thermal stability of asphalt binder directly affects the degree of thermal decomposition of asphalt, especially the asphalt binder as the main material of highway construction, when the vehicle fire on the pavement, asphalt binder will produce pyrolysis reaction, which will cause the destruction of the pavement structure and release a large amount of heat, which is easy to cause casualties [17,18]. Therefore, the study of thermal stability and pyrolysis mechanism of asphalt binder has important theoretical significance and practical application value.

In recent years, the thermal stability and pyrolysis mechanism of asphalt binder has become a hot research topic. Many scholars [19–22] have used advanced experimental techniques, such as thermogravimetric analysis (TGA), differential scanning calorimetry (DSC), or thermogravimetric-Fourier transform infrared spectroscopy (TG-FTIR), to investigate the thermal stability of asphalt in depth. Generally speaking, the decomposition temperature of asphalt is defined between 200 °C and 350 °C, and the decomposition temperature directly reflects the thermal stability of asphalt, the higher the decomposition temperature means the stronger the thermal stability of asphalt.

Regarding the pyrolysis mechanism of asphalt, researchers have used a variety of kinetic methods to study it. For example, Hao [23] determined the thermal-cracking kinetic parameters of oil sand bitumen using the iso-conversional Friedman procedure, and the activation energy of oil sand bitumen ranging from 93.74 to 215.99 kJ/mol in the whole pyrolysis process. Tan [24] found that the pyrolysis of asphalt binder with composite fire retardant is a single-stage thermal decomposition reaction by non-isothermal pyrolysis kinetics, and the higher heating rate causes asphalt binder to release more heat and gaseous products. Ren [25] analyzed waste crumb rubber modified asphalt binder with different swelling-degradation by Flynn-Ozawa-Wall (FOW) and Kissinger-Akahira-Sunose (KAS) kinetic methods, and it was found that swelling CRMB binder and degradation CRMB binder have very different pyrolysis mechanisms. These studies suggest that different types of asphalt binder or the same type of asphalt binder may exhibit different models of pyrolysis mechanisms at different temperatures. However, it is worth noting that there have been a large number of studies focusing on the pyrolysis reaction mechanism of conventional asphalt, but there is a lack of research on the pyrolysis reaction mechanism of SBS/TB crumb rubber modified asphalt binder. In order to improve the research on SBS/TB crumb rubber modified asphalt binder, it is necessary to further investigate its pyrolysis characteristics, so as to provide theoretical support for related engineering applications.

This study mainly aims to investigate the micro-modification mechanism, thermal stability and rheological properties, and to explore the pyrolysis mechanism and the correlation between microstructural, thermodynamic and rheological parameters of SBS/TB crumb rubber modified asphalt binder. To this end, SBS/TB crumb rubber modified asphalt binder with different dosage was prepared in this study. The modification mechanism of SBS/TB crumb rubber modified asphalt was analyzed by fluorescence microscopy (FM) and Fourier transform infrared (FTIR). And the thermal stability of SBS/TB crumb rubber modified asphalt binder was characterized by TG analysis and its pyrolysis mechanism was analyzed by kinetic methods. In addition, Dynamic Shear Rheometer (DSR) and Bending beam rheometer (BBR) were used to evaluate and analyze the rheological properties, high-and-low temperature performance.

2. Materials and methods

2.1. Raw materials

In this study, SK70# petroleum asphalt was selected as fresh binder, and its basic technical specifications are shown in Table 1. Crumb rubber derived from waste car tires with a particle size of 80 mesh was used and its technical specifications are shown in Table 2. The linear SBS polymer base was T161B produced by Dushanzi Petrochemical Company in Xinjiang, China, with a block ratio of 30:70. Its basic technical parameters are presented in Table 3.

2.2. Preparation of modified asphalt binder

In this study, terminal blend technology was employed to desulfurize or depolymerize the rubber particles in the asphalt binder to ensure their adequate dispersion. The specific preparation process is illustrated in Fig. 2.

The abbreviated names of the samples for various proportions are explained in Table 4.

Table 1
Basic properties of SK70# Petroleum asphalt.

Test		Values	Standard requirements	Testing method
Penetration at 25 °C/mm		67	60–80	T 0604–2011
Softening point/°C		52.5	≥ 46	T 0606–2011
Ductility at 15 °C		> 100	≥ 100	T 0605–2011
Density at 15 °C /(g cm^{-3})		1.037	Record of actual measurements	T 0603–2011
Viscosity at 135 °C/(Pa s)		2.608	≤ 3	T 0619–2011
Thin film oven test (TFOT)	Quality loss/%	−0.504	−0.8 ~ 0.8	T 0610–2011
	Penetration ratio/%	72	≥ 61	T 0604–2011
	Residual ductility at 15 °C/cm	20	≥ 15	T 0605–2011

Table 2
Crumb rubber basic technical parameters.

Technical Item	Test Result	Technical Requirements
Relative Density	1.18	/
Heating Loss	0.38 %	≤ 1.0 %
Acetone Extractables	7 %	≤ 14 %
Carbon Black Content	30 %	≥ 28 %
Rubber Hydrocarbon Content	56 %	≥ 48 %
Fiber Content	0.02 %	≤ 0.5 %
Metal Content	0.01 %	≤ 0.03 %

Table 3
T161B linear SBS technical parameters.

Technical Item	Test Result	Unit
Oil Content	0	wt%
Styrene Content	31	wt%
Volatile Content	0.38	wt%
300 % Tensile Stress	2.41	MPa
Tensile Strength	25.4	MPa
Elongation at Break	750	%
Shore Hardness	79	Shore A

2.3. Test and evaluation methods

2.3.1. Fluorescence microscopy test

In this study, fluorescence microscopy (FM) was used to observe the micro-morphological characteristics of each modified asphalt binder under 200 x magnification to analyze and evaluate the dispersion effect of the polymers and their compatibility with the asphalt binder.

2.3.2. Segregation test

The storage stability of modified asphalt binder is commonly evaluated by standard tube separation tests, which can well reflect the compatibility between modifier and asphalt binder. The modified asphalt binder was loaded into the dissociation tube and then put into the oven at 163 ± 0.5 °C for a certain period. Putting the release tube into the freezer to freeze solid, and taking 1/3 of the asphalt binder from the top and bottom of the pipe respectively for softening point test.

2.3.3. Fourier infrared spectroscopy test

During the test, the samples were covered on the surface of the ATR reflector crystals respectively and fixed with metal so that the asphalt binder was in complete contact with the diamond, and 32 scans were performed for each sample in the wave number range of 4000–400 cm^{-1} with a resolution of 4 cm^{-1}.

2.3.4. Thermogravimetric Analysis

Thermogravimetric Analysis (TGA) method was used to analyze the thermal stability of each modified asphalt binder specimen, the samples were in a nitrogen atmosphere throughout the test, with a sample mass of about 10 mg, and the temperature range was from 30 °C to 700 °C, with the temperature increase rate set at 10 °C/min.

2.3.5. PG classification test

Testing of modified asphalt binder specimens by PG grading program. The initial temperature of the test was 64 °C, the warming interval was 6 °C, the shear strain was 12 %, and the loading frequency was 10 rad/s. The change in rutting factor (G*/sin δ) of each modified asphalt binder specimen was recorded, and the high temperature failure temperature of each modified asphalt binder was analyzed.

2.3.6. Frequency sweep test

In the frequency sweep test program, parallel plates of 25 mm were selected for the test rotor, the zero clearance of the parallel plates was 1 mm, the frequency range of the load action was 0.1–100 Hz, the temperature range was 30–80 °C with an increase of 10 °C, and the shear strain value was controlled as 0.1 %. Master curve and Han curve plotted from frequency sweep results.

2.3.7. Zero-shear viscosity measurement

In this paper, the frequency scanning program in DSR was selected to determine the zero-shear viscosity of modified asphalt binder samples under different shear rates. The test temperature is selected as 60 °C, the scanning range of shear rate is selected as 0.01–100 rad/s, the loading mode is selected as strain-controlled loading, and the loading strain is set at 1 %.

2.3.8. Multiple stress creep and recovery test

The Multiple stress creep and recovery (MSCR) test was used to evaluate the permanent deformation resistance and elastic recovery properties of modified asphalt binder. In this study, all asphalt binder samples were subjected to rolling thin film oven (RTFO) short-term aging treatment, and the aging specimens were tested using the DSR stress recovery control mode according to AASTO TP70-09 standard. The test temperatures were 64 °C, 70 °C, and 76 °C, and two stress levels of 0.1 kPa and 3.2 kPa were applied, of which 20 creep (1 s)-recovery (9 s) cycles were performed at the 0.1 kPa stress level, and 10 cycles were performed at the 3.2 kPa stress level for a total of 300 s.

Table 4
Abbreviations of samples.

Sample Name	Description
S_2	2 % SBS Modified asphalt binder
S_3	3 % SBS Modified asphalt binder
S_2R_{10}	2 % SBS and 10 % TB Crumb Rubber Composite Modified asphalt binder
S_2R_{15}	2 % SBS and 15 % TB Crumb Rubber Composite Modified asphalt binder
S_3R_{10}	3 % SBS and 10 % TB Crumb Rubber Composite Modified asphalt binder
S_3R_{15}	3 % SBS and 15 % TB Crumb Rubber Composite Modified asphalt binder

Fig. 2. Preparation process of SBS/TB crumb rubber modified asphalt binder.

2.3.9. Bending Beam Rheometer test

This study used the BBR-1 for the test. The test specimens were selected from RTFO aged asphalt binder, respectively, held at the corresponding test temperatures (-12 °C, −18 °C, −24 °C) for 1.5 h and then applied a constant load of 980 mN ± 50 mN to the asphalt binder beams in accordance with the AASHTO T313-08 specification [26] and the instrument operating procedures for a duration of 240 s, and outputted through the computer the corresponding creep strength S and creep rate m.

3. Results and discussion

3.1. Microscopic modification mechanism

The asphalt binder specimens in this study were observed at a magnification of 200 times, and the fluorescence microscopy images obtained from the tests are shown in Fig. 2 It can be found in the base asphalt binder and polymer modifier different fluorescence properties lead to the two phases in the miscible system shows obvious color

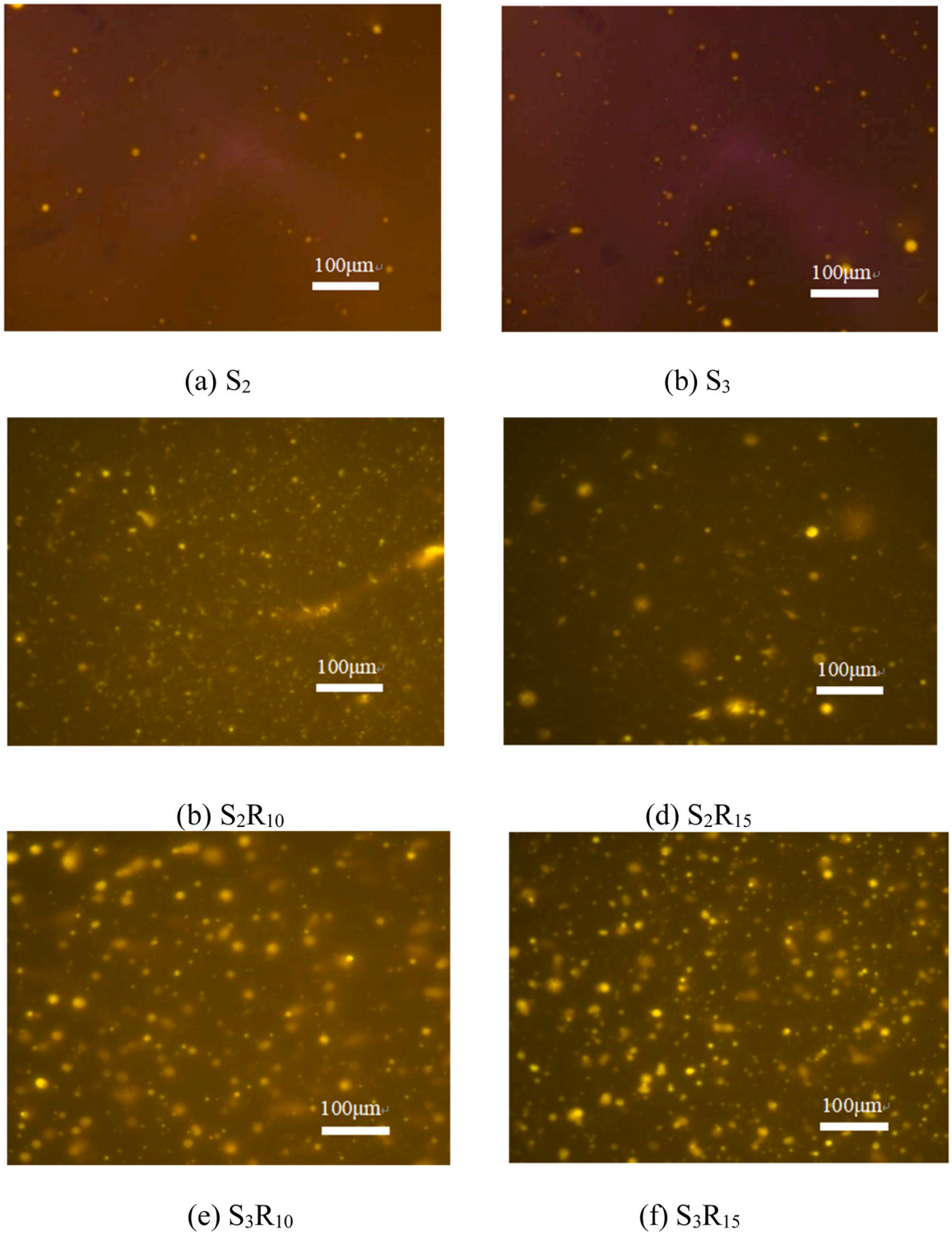

Fig. 3. Modified asphalt binder fluorescent microscopic images.

differences, in which the brighter fluorescent spots for a variety of modifier particles. Each modifier particles in the asphalt binder base shows independent of each other, dispersed more uniform morphology, which indicates that SBS and TB crumb rubber as a dispersed phase can be uniformly distributed in the continuous phase of asphalt binder, and the two have better compatibility, indirectly verifying the rationality of the modification process used in this paper.

Comparing the images of SBS/TB crumb rubber modified asphalt binder and single SBS modified asphalt binder, it can be found that the number of fluorescent dots increased significantly after the addition of TB crumb rubber, and the number of particles with larger diameter has been improved, the main reason is that under the action of high-temperature shear, the TB crumb rubber particles absorbed asphalt binder components partially dissolved, and the size of the particles increased [13]. It is worth noting that for the four SBS/TB crumb rubber modified asphalt binders, their fluorescence images show no crosslinked mesh structure as the traditional SBS/crumb rubber modified asphalt binder, which is attributed to the fact that the dissolution mechanism of TB crumb rubber is different from that of the ordinary crumb rubber, and the TB powder particles are desulphurized or depolymerized in the hot asphalt binder, and thus well dispersed in the blends.

In this study, Image Pro-Plus: IPP was used to obtain the micro-morphological parameters of the polymer phase and to quantify the dispersion of the high viscosity modifier in the asphalt binder using two evaluation metrics, namely, polymer particle area shares and particle size distribution (PSD). Firstly, the image in Fig. 3 needs to be binarized, and the results are shown in Fig. 4 Then the relevant shape parameters of the corresponding contour lines of asphalt binder and modifier particles in the binarized image were extracted separately to obtain the fluorescent particle area share and PSD statistics of different modified asphalt binder, as shown in Fig. 5(a) and (b), respectively.

Combining the results of the two figures, it can be seen that the area share of SBS/TB crumb rubber composite modifier is significantly higher than that of SBS modifier, and the concentrated distribution of particle size is large. On the one hand, it is due to the larger total dosage of composite modifier, on the other hand, it also shows that the dosage of TB crumb rubber enhances the degree of compatibility between SBS and asphalt binder, and the modification effect is more favorable. In addition, it can be noted that the area of the S_3R_{10} the S_3R_{15} polymer phase is increased 4–5 times and the particle size distribution is denser, which

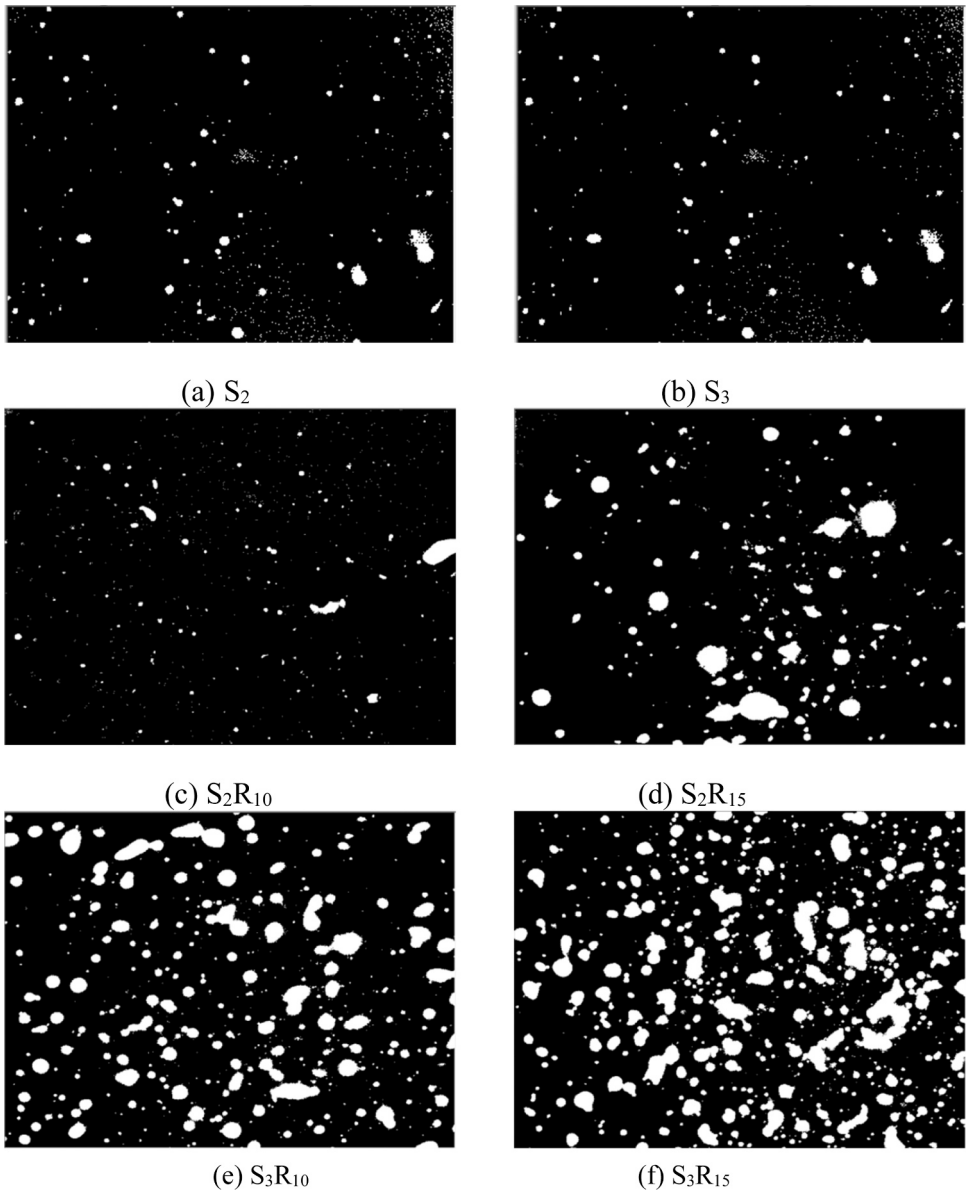

Fig. 4. Results of the binarization of the fluorescence microscopy images.

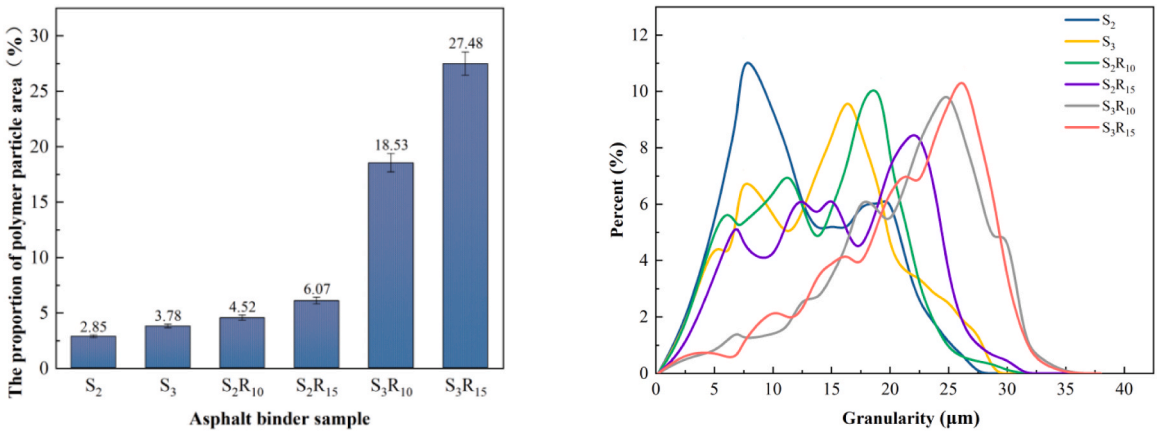

(a) Polymer particle area ratio (b) Average particle size distribution

Fig. 5. Results of polymer phase treatment. Note 1: Area% represents the percentage of absorption peak area, Mp represents the peak molecular weight, and D is the dispersion of the absorption peak.

indicates that the composite modifier at these doping levels are more uniformly dispersed, and is less prone to agglomeration. As far as the modification effect is concerned, the modified combination of 3 % SBS and TB crumb rubber can be considered as the best blending ratio in the experimental group shown.

3.2. Storage stability

The difference between the softening points of the top and bottom parts is to evaluate the storage stability performance of the modified asphalt binder. According to specifications, the softening point difference at 48 h is not allowed to exceed 2.5 °C. Fig. 6 illustrates the softening point differences between the top and bottom samples of aluminum pipes following segregation for each modified asphalt binder sample. The results indicate that the softening point difference for the SBS modified asphalt binder fails to meet the specification requirement of being less than 2.5 °C. In contrast, the SBS/TB rubber crumb modified asphalt binder adheres to the specified criteria.

This is mainly because the low mixing amount of TB crumb rubber and SBS can better form a uniform cross-linked network structure and improve the storage stability of asphalt binder. However, the high amount of TB rubber powder will aggravate the agglomeration and

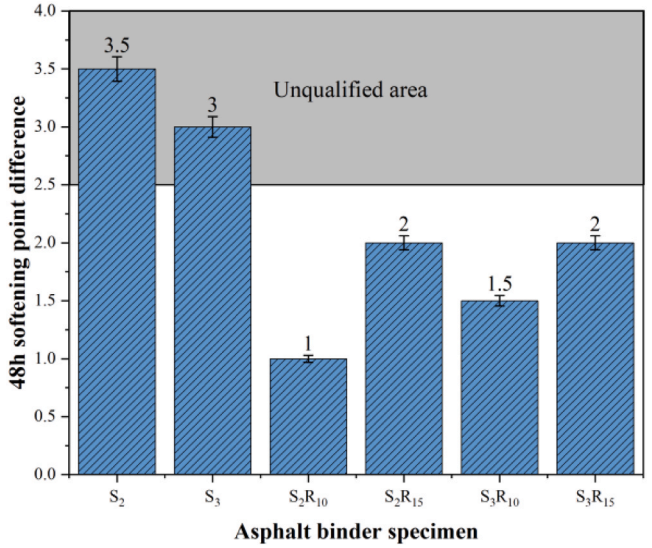

Fig. 6. Results of the softening point difference test.

entanglement between the compound modifying agents, which leads to the increase of the heterogeneity of the modified asphalt binder system and the decrease of the storage stability.

3.3. FTIR

The results of the infrared spectra of each modifier, each modified asphalt binder and the functional groups corresponding to the characteristic absorption peaks are shown in Fig. 7 and Table 5. As can be seen in Fig. 7, the infrared characteristic absorption peaks of unaged base asphalt binder are mainly distributed at wave numbers of 3400 cm^{-1}, 2920 cm^{-1}, 2850 cm^{-1}, 1600 cm^{-1}, 1455 cm^{-1}, 1375 cm^{-1} and 1032 cm^{-1}, according to the corresponding functional group information in Table 5, it can be seen that most of these strong absorption peaks are the result of the C-H vibration of cycloalkanes and alkanes in the base asphalt binder molecule, indicating that hydrocarbons are contained in the molecular composition of base asphalt binder, and the conjugated double-bond absorption peaks appearing at 1600 cm^{-1} indicate that aromatic compounds are also present in the base asphalt binder.

As Fig. 7(a) shows the main absorption peaks of CR and SBS are similar, mainly the stretching vibration of -CH_3 and -CH_2-, and other groups. And as can be seen in Fig. 7(b), compared to BA, the IR spectra of S_2 and S_3 show obvious absorption peaks at 966 cm^{-1} and 699 cm^{-1}, which is the result of the C-H vibration effect on the carbon-carbon double bond of the polybutadiene segment and on the benzene ring of the polystyrene segment in the SBS composition. And compared with BA, the IR spectra of S_2 and S_3 show obvious absorption peaks at 966 cm^{-1} and 699 cm^{-1}, which is the result of the C-H vibrational interactions on the carbon-carbon double bond of the polybutadiene segment and on the benzene ring of the polystyrene segment in the SBS composition.

Fig. 7(c) shows the infrared spectral characteristics of modified asphalt binder composite with different dosage of SBS/TB crumb rubber. Comparing S_2 and S_3 in Fig. 7(b), the infrared characteristic absorption peaks of SBS/TB binder composite modified asphalt binder are also located at 966 cm^{-1} and 699 cm^{-1} wave numbers, and there are no new characteristic absorption peaks appeared or disappeared, but the intensity of the absorption peaks at the wave numbers of 1600 cm^{-1}, 1455 cm^{-1}, 1375 cm^{-1}, 966 cm^{-1} and 699 cm^{-1} is weakened and the significance of this weakening effect is positively correlated with the blending amount of TB crumb rubber, this indicates that in the process of SBS and TB crumb rubber composite modification, mainly the conjugated double bonds on the benzene ring, -CH_3, -CH_2-, -C═C- and C-H on

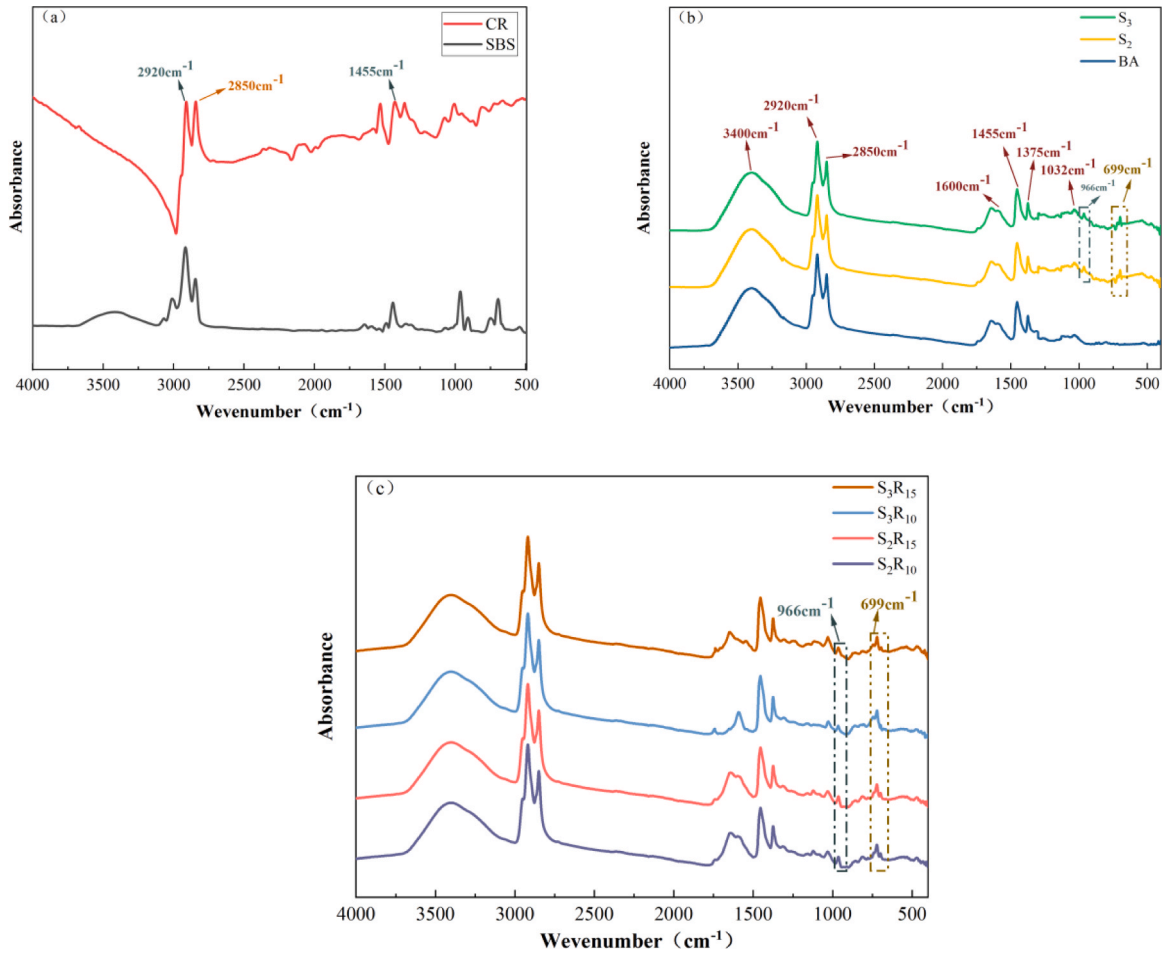

Fig. 7. Infrared spectroscopy of various modifier, base asphalt binder and various modified asphalt binder.

Table 5
The absorption peak position of the infrared spectrum and the corresponding functional groups.

Absorption peak position/ cm^{-1}	Functional groups and vibration type
3400	Expansion vibration of -OH
2920	$-CH_2-$ of the anti-of ic vibration
2850	Symmetric telescopic vibration of $-CH_2-$
1600	Conjugated double bond (Phenyl ring skeleton vibration)
1455	C-H plane expansion vibration in CH_3 (Variant Angle vibration)
1375	The ic vibration in the C-H surface in-CH_2- (flexural vibrations)
1032	Sulfoxide -S═O
966	Polybutyl diene segment -C═C-
813	Bending vibration outside the C-H surface on the benzene ring
699	C-H vibration on the benzene ring of the polystyrene segment

the benzene ring undergo a chemical reaction, in which the intensity of the absorption peak located at 966 cm-1 (-C═C-) has the most obvious change, which is due to the fact that the -C═C- is unstable and easy to be opened during the process of heating and shear, and it has a stronger activity after being opened, so as to undergo a branching reaction with the crumb rubber.

3.4. TGA/DTG analysis

Fig. 8 shows the TGA and DTG curves of each modified asphalt binder, respectively. From Fig. 8(a), it can be seen that the mass of asphalt binder is almost constant until 200 °C, and when the temperature exceeds 200 °C, the mass of asphalt binder decreases rapidly as the temperature increases, and after the temperature exceeds 550 °C, the asphalt binder quality decreases slowly until it stops. Between 200 °C and 550 °C, asphalt binder undergoes pyrolysis. Fig. 8(b) shows the decomposition rate of different modified asphalt binders at different temperatures, the pyrolysis rate of each modified asphalt binder is different, but the overall trend is first fast and then slow, and there is only one peak value.

Table 6 lists the pyrolysis parameters of different modified asphalt binders, including the pyrolysis start temperature Ts, maximum DTG value DTG_{max}, corresponding temperature T_{DTGmax}, and residue percentage Re. Increased amounts of SBS and TB crumb rubber will increase the decomposition temperature of asphalt binder compared to S_2, this is due to the formation of a denser mesh between the asphalt binder, SBS and TB crumb rubber hindering the pyrolysis reaction. Meanwhile, the Re of the modified asphalt binder increased with the increase of TB crumb rubber dosage, which further indicates that the compound modification of SBS and TB crumb rubber can improve the thermal stability of asphalt binder. In addition, the T_{DTGmax} of various modified asphalt binders do not differ much, but the corresponding DTG_{max} varies considerably, due to the fact that TB crumb rubber absorbs some of the oil in the asphalt binder, when the temperature reaches T_{DTGmax}, the TB crumb rubber and the absorbed oil are simultaneously pyrolyzed, resulting in a larger DTG_{max}.

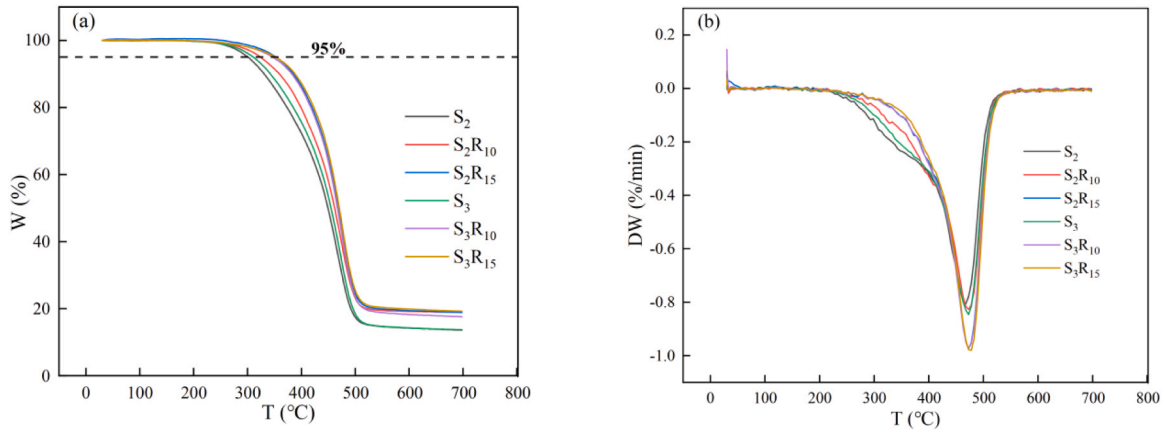

(a) TGA curve (b) DTG curve

Fig. 8. TGA/DTG analysis.

Table 6
The pyrolysis parameters of different modified asphalt binders.

Sample name	T_S (°C)	DTG_{max}(wt%/°C)	T_{DTGmax}(°C)	Re(%)
S_2	298.13	0.81	467	13.59
S_3	313.13	0.84	472	13.71
S_2R_{10}	323.12	0.82	472	18.87
S_2R_{15}	348.06	0.97	472	18.93
S_3R_{10}	353.16	0.97	477	17.56
S_3R_{15}	353.05	0.98	477	19.21

Note 2: T_S is defined as the temperature at which five percent of the mass is lost.

In order to investigate the pyrolysis kinetic parameters of SBS/TB crumb rubber modified asphalt binder as well as the mechanism model, pyrolysis kinetic analysis of six modified asphalt binders was carried out. Because the kinetic mechanism of pyrolysis of the specimens is unknown, the Flynn-Ozawa-Wall (FOW) and Kissinger-Akahira-Sunose (KAS) treatments [27], which do not require consideration of the reaction mechanism, were used. This can avoid some errors caused by different assumptions of the reaction mechanism function and make the calculation results closer to the actual situation. The formulae for the two treatments are shown in Eqs. (1) and (2):

$$\lg \beta = \lg \frac{AE}{Rg(\alpha)} - 2.315 - 0.4567\frac{E}{RT} \quad (1)$$

$$\ln \frac{\beta}{T^2} = \ln \frac{AR}{g(\alpha)} - \frac{E}{RT} \quad (2)$$

Eq. (1) is the FOW equation and Eq. (2) is the KAS equation. Where, β is the heating rate, °C/min, A represents the pre-exponential factor, min^{-1}, Ea is the activation energy, kJ/mol, and R refers to the gas constant, 8.314 J mol^{-1} K^{-1}, α is the conversion rate, T is the temperature, K.

The g(a) is a model of the kinetic mechanism of the pyrolysis process. For the FOW, lng(a) is linearly related to 1/T, for the KAS, lng(a) and T satisfy the equation form y = a+ 2lnx-b/x. The form of g(α) in common thermal reaction models is shown in Table 7.

The conversion rate α is calculated as shown in Eq. (3):

$$\alpha = \frac{(m0 - mt)}{m0 - m\infty} \quad (3)$$

Where m_0 is the initial mass of the reaction, m_t is the sample mass at time t, and m_∞ is the residual mass of the reaction.

In the kinetic calculation of the weight loss process of the sample, there is only one weight loss peak, so the entire pyrolysis process is considered as a single reaction stage. Considering the special nature of asphalt binder thermal decomposition, there is a deviation between the induction zone in the early stage of the reaction process and the coking period in the late stage of the reaction to reflect the true pyrolysis process. Therefore, $0.1 \leq \alpha \leq 0.9$ was selected as the analysis interval for the study.

Table 7
Common solid-state thermal reaction models.

Reaction mechanism	Code	g(α)
First order	F1	-ln(1-α)
Second order	F2	$(1-\alpha)^{-1}-1$
Third order	F3	$[(1-\alpha)^{-1}-1]/2$
One-dimension diffusion	D1	α^2
Two-dimension diffusion	D2	(1-α)ln(1-α)+α
Three-dimension diffusion	D3	$[1-(1-\alpha)^{1/3}]^2$
Four-dimension diffusion	D4	$1-2\alpha/3-(1-\alpha)^{2/3}$
Two-dimension nucleation	A2	$[-\ln(1-\alpha)]^{1/2}$
Three-dimension nucleation	A3	$[-\ln(1-\alpha)]^{1/3}$
One-dimension phase boundary	R1	α
Contracting sphere	R2	$1-(1-\alpha)^{1/2}$
Contracting cylinder	R3	$1-(1-\alpha)^{1/3}$

The FOW and KAS equations were used respectively and combined with Table 7 to fit the relationship between conversion rate a and temperature T. The fitted curves are shown in Figs. 9 and 10. It can be seen that the fitted curves correspond well to the real data, and the FOW and KAS equations as well as thermal reaction models can fit the kinetic curves well. The calculated results of Ea, A and correlation coefficient R^2 corresponding to each modified asphalt binders are listed in Figs. 11 and 12.

It can be seen that R^2 are all greater than 0.90, further indicating that the fitting effect of different models is good, which verifies the reliability of the dynamic model calculation, However, there are still differences in the corresponding R^2 under different models. Choose the three thermal reaction models with R^2 closest to 1. When using the FOW equation, for S_2 and S_2R_{10}, D1, R1, R2 are better for S_2R_{15}, D1, D4, R1 are better for S_3, S_3R_{10} and S_3R_{15}, D1, D2, R1 are better. When using the KAS equation, for S_2, S_2R_{10}, S_2R_{15}, S_3 and S_3R_{10} are better, for S_3R_{15}, D1, A3, R1 are better. D1 and R1 have the best fitting effects on SBS/TB crumb rubber modified asphalt binder with different dosages, and the D1 and R1 were ultimately chosen for subsequent analysis.

It can be seen that the Ea and A trends of D1 and R1 are the same from Figs. 11 and 12. The activation energy Ea represents the energy required to change a asphalt binder molecule from its normal state to an active state in which chemical reactions can easily take place, and the

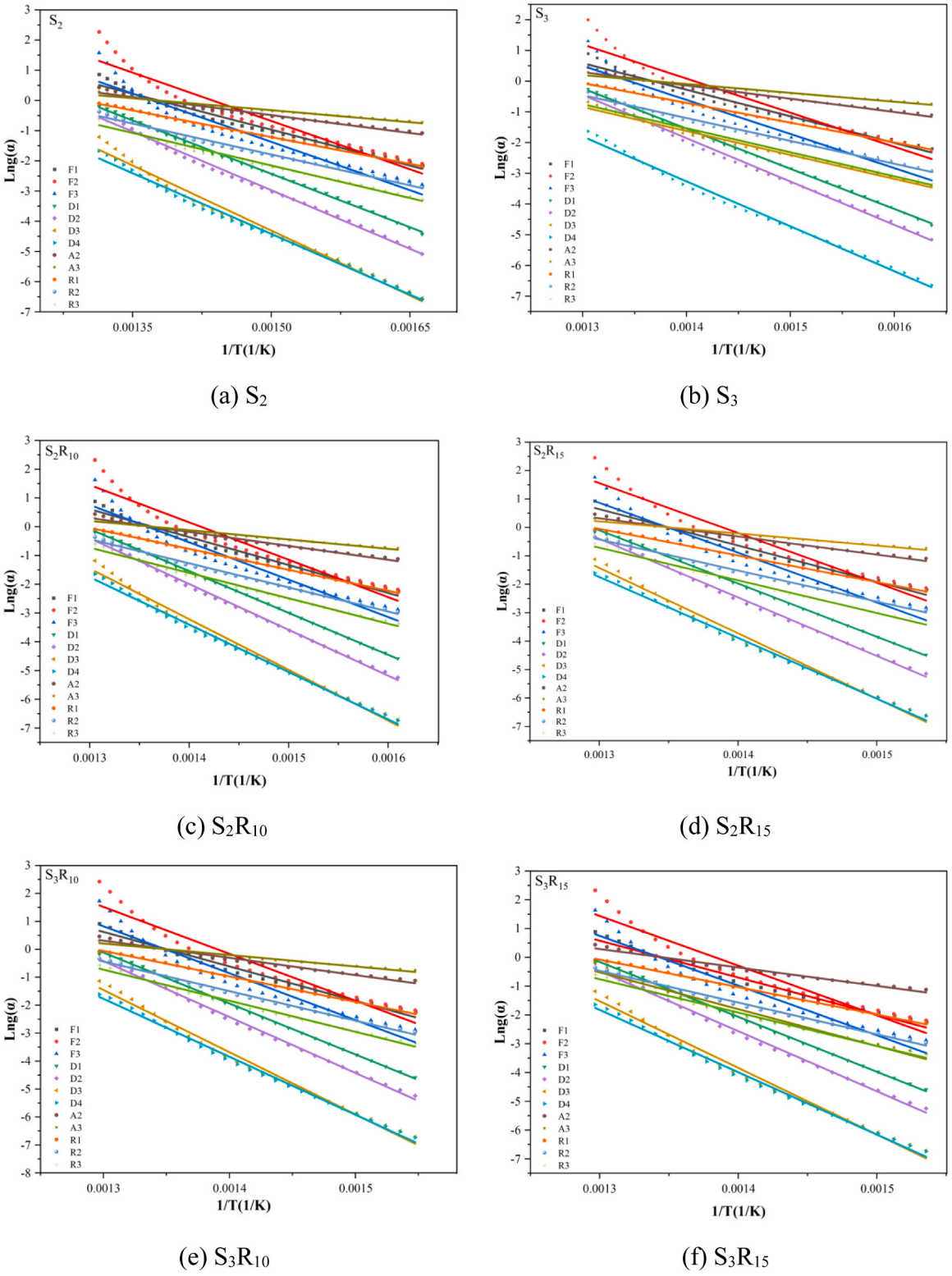

Fig. 9. The kinetic analysis of SBS/TB crumb rubber asphalt binder using FOW.

higher the activation energy, the lower the number of activated molecules and the lower the degree of reaction [21]. The pre-exponential factor A reflects the number of times asphalt binder molecules collide and initiate a chemical reaction. It can be seen that with the increase of SBS and TB crumb rubber blending, Ea and A show an overall upward trend.

This is because a stable three-dimensional network structure forms within the asphalt binder due to strong cross-linking interactions between TB crumb rubber and SBS, lengthening the path for heat to penetrate the asphalt binder interior. And then, TB crumb rubber restricts the migration of asphalt binder molecules and reduces the heating rate of asphalt binder materials, so the activation energy and thermal stability of SBS/TB crumb rubber modified asphalt binder are higher.

The basic thermodynamic parameters the enthalpy (ΔH), Gibbs free

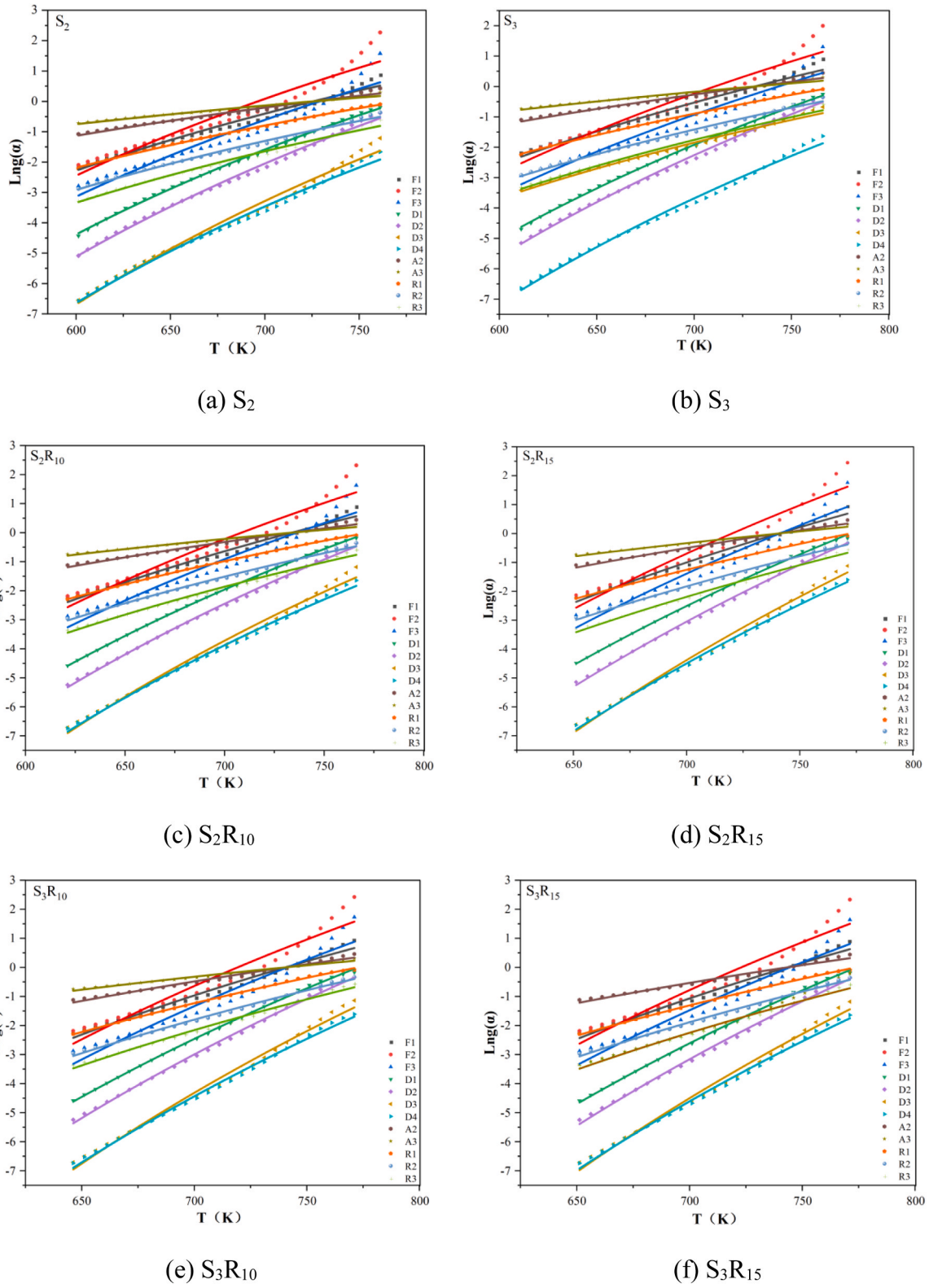

(a) S_2 (b) S_3

(c) S_2R_{10} (d) S_2R_{15}

(e) S_3R_{10} (f) S_3R_{15}

Fig. 10. The kinetic analysis of SBS/TB crumb rubber asphalt binder using KAS.

energy (ΔG), and entropy (ΔS) represent the state functions of heat released or absorbed, chemical bond dissociation, and system energy change, respectively, for a given condition. The formulas are as follow Eqs. (4)–(6). In this paper, the D1 of the FOW equation was chosen as an example to calculate ΔH, ΔG, and ΔS for six modified asphalt binder samples, and the results are shown in Table 8.

$$\Delta H = Ea - RT \tag{4}$$

$$\Delta G = Ea + RT \max \ln\left(\frac{KBT \max}{hA}\right) \tag{5}$$

$$\Delta S = (\Delta H - \Delta G)/T \max \tag{6}$$

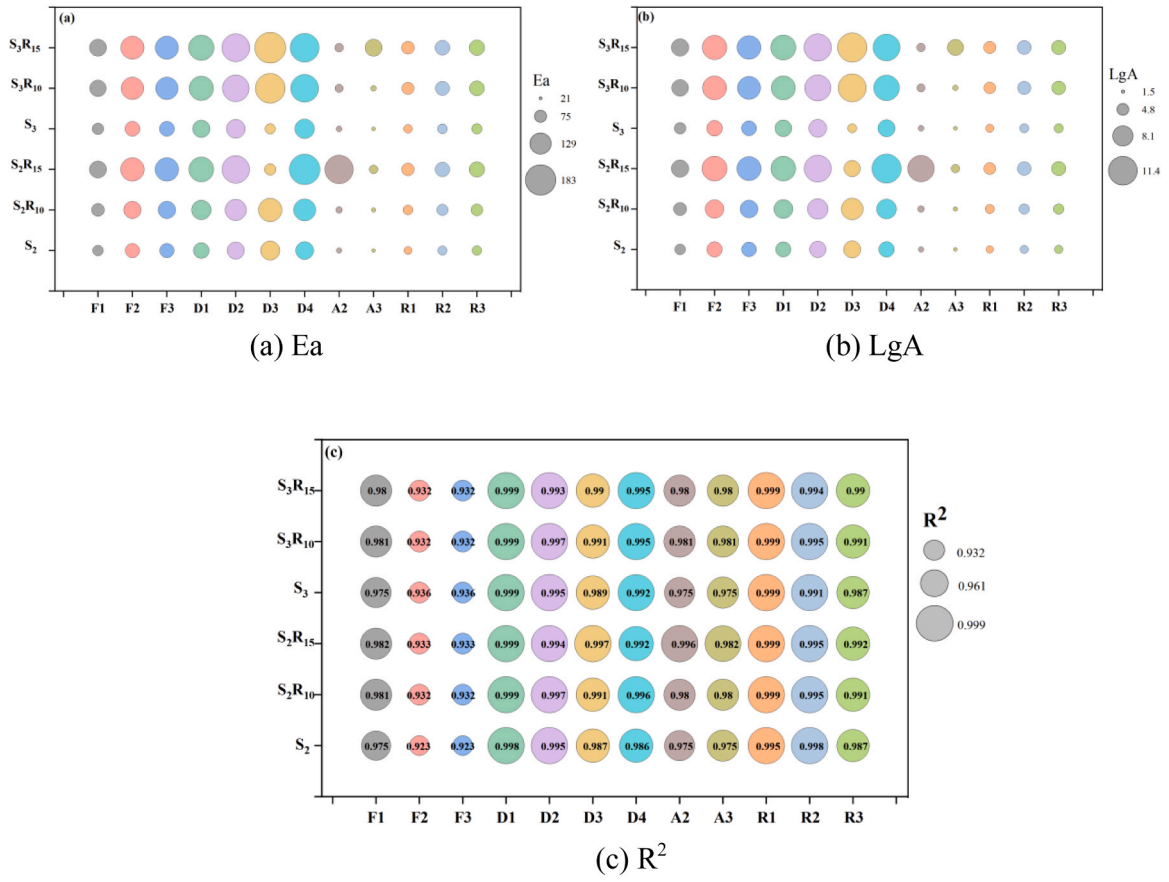

Fig. 11. Bubble plots of kinetic parameters of SBS/TB rubber-modified asphalt binders determined by the FOW method.

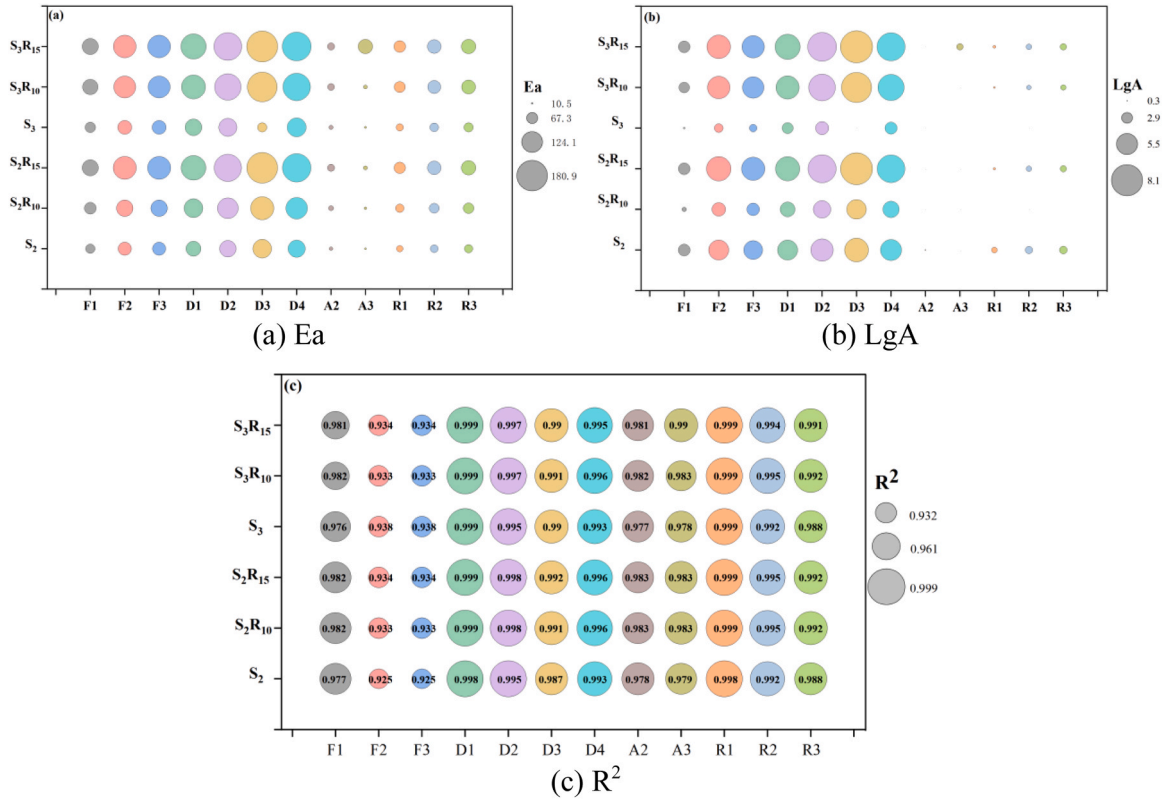

Fig. 12. Bubble plots of kinetic parameters of SBS/TB rubber-modified asphalt binders determined by the KAS method.

Where the Ea and A are both obtained from kinetic models, K_B is the Boltzmann constant ($1.381*10^{-23}$J K^{-1}), and h refers to the Planck's constant, $6.626*10^{-34}$J s^{-1}.

A positive value of ΔH indicates that pyrolysis of modified asphalt binder requires the absorption of heat thereby breaking the chemical bonds for the reaction to take place. In addition, the trend of ΔH is consistent with the activation energy, and the difference between ΔH and Ea of the modified asphalt binder is very small, which indicates that the thermal reaction is possible and that the thermal reaction is mainly facilitated by exogenous energy. For ΔG, six modified asphalt binders showed positive values, indicating that the pyrolysis reaction is not likely to proceed spontaneously, and additional energy needs to be externally applied to promote the thermal reaction of the modified asphalt binder. ΔS was negative for six modified asphalt binders, indicating a lower degree of disorder in the pyrolysis process of modified asphalt binder for the products than for the reactants. And with the increase of SBS and TB crumb rubber doping, there is an overall upward trend in the degree of ordering of the reactants.

3.5. Rheological performance analysis of composite modified asphalt binder

3.5.1. Analysis of master curve

The time course of the master curve is not the true course of the experimental measurement, and is usually referred to as the conversion time, and the distance shifted parallel to the axis of the conversion time is called the shift factor α of the temperature corresponding to the reference temperature, obtained by fitting the Williams Landel Ferry (WLF) equation (Eq. (7)), and the complex shear modulus and phase angle principal curves constructed according to the time-temperature superposition principle were fitted by the Sigmoid function model [28], As shown in Eqs. (8) and (9).

$$\log \alpha(T) = \frac{-C_1(T - T_0)}{[C_2 + (T - T_0)]} \tag{7}$$

$$\log |G*|_{\text{fit}}(f_r) = \log |G*|_{\min} + \frac{\log |G*|_{\max} - \log |G*|_{\min}}{1 + e^{\beta+\gamma(\log f + \log \alpha_{(T)})}} \tag{8}$$

$$\delta = \frac{-90\alpha_{(T)}\gamma e^{\beta+\gamma(\log f + \log \alpha_{(T)})}}{(\beta + \gamma(\log f + \log \alpha_{(T)}))^2} \tag{9}$$

Where α(T) is the displacement factor with respect to the reference temperature at temperature T, T_0 is the reference temperature, f_r is the reduced frequency (Hz) at the reference temperature, f is the frequency (Hz) at the test temperature, $|G^*|_{\text{fit}}$ is the complex shear modulus obtained from the fit, $|G^*|_{\max}$ and $|G^*|_{\min}$ are the complex modulus (Pa) maximum and minimum values, respectively, δ is the phase angle obtained from the fit, and C_1, C_2, α, δ, β, and γ are model coefficients.

30 °C was selected as the reference temperature for plotting the master curve, and the results of the displacement factors and model parameters calculated for each asphalt binder sample are shown in Table 9. The corresponding complex modulus and phase angle master curves are shown in Fig. 13. From Fig. 13(a), it can be seen that the increase of the reduction frequency leads to the increase of the complex modulus, and in the low-frequency domain, there is a large difference in the complex shear modulus of the specimens, but in the high-frequency domain, the complex modulus tends to be the same in all the binders. This is because when the loading frequency is too high, the asphalt binder exhibits a flow behavior that approximates a pure fluid, and the percentage of elastic components is reduced to a minimum. In addition, it can be found that S_2 has the smallest strength in the same temperature and frequency range, compared to the increase in the complex modulus curve of the asphalt binder specimens by increasing the dosage of both SBS and TB crumb rubber, which implies an increase in the strength of the specimens.

From Fig. 13(b), it can be seen that the phase angle of each specimen shows an approximately linear decrease with the increase of the curtailment frequency, with the phase angle of S_2 being the largest and that of S_3R_{15} being the smallest. The addition of both SBS and TB crumb rubber leads to a downward shift in the phase angle curve, suggesting that both polymers improve the stiffness and elasticity of the asphalt binder, while having difficulty exhibiting shear hysteresis effects. And it is worth noting that in the same reduced frequency range, compared with other specimens, the phase angle change of S_2R_{10} is larger, and the phase angle is more likely to increase under low-frequency conditions, and combined with the time-temperature equivalence principle of low-frequency corresponds to high-temperature principle to infer that S_2R_{10} is more prone to flow deformation under high-temperature conditions.

Table 8
Thermodynamic parameters of SBS/TB crumb rubber modified asphalt binder calculated by FOW-D1 method.

Simple name	ΔH (kJ/mol)	ΔG (kJ/mol)	ΔS (J/mol K)
S_2	89.331	156.632	−144.112
S_3	99.436	162.012	−132.57
S_2R_{10}	111.201	166.006	−116.111
S_2R_{15}	144.000	178.689	−73.492
S_3R_{10}	140.073	177.661	−78.801
S_3R_{15}	146.842	180.361	−70.269

3.5.2. Analysis of Han curve

The Han curve is a curve that describes the relationship between the logarithm of the storage modulus (logG') and the logarithm of the loss modulus (logG'') of a homogeneous polymer, reflecting the microstructural changes of the polymer during oscillatory shear at small strains [29]. And then Han et al. proposed a pipeline model to describe the similarity of chemical structures in polymer blends to predict the effect of polydispersity on the logG' versus logG'' curves of linearly crosslinked homopolymers in the end region, as shown in Eq. (10). For linearly crosslinked homopolymers, the slope of the end region of the logG' versus logG'' relationship curve is equal to 2. However, for polymers with polydispersity, the slope is less than 2 (Eq. (11)). In general, the value of this slope for modified asphalt binder samples is less than 2.

$$\log G' = 2\log G'' + \log\left(1.2G_N^0\right) + 3.4\log\left(\frac{M_Z}{M_W}\right) \tag{10}$$

$$\log G' = x\log G'' + \left(1 - x\right)\log\left(8\frac{G_N^0}{\pi^2}\right) \tag{11}$$

Where G' is the storage modulus (Pa), G'' is the loss modulus (Pa), G_N^0 is the modulus of the plateau region, M_Z and M_W are the number-averaged molecular weight and the weight-averaged molecular weight, respectively, and x is the slope of the logG' versus logG'' curve.

Fig. 14 shows the composite modified asphalt binder samples Han curve, from the figure can be seen in this study prepared high viscosity asphalt binder phase separation critical temperature of about 70 °C, and by comparing all the specimens of the "Han" curve can be found, the temperature exceeds 70 °C, the phase separation phenomenon is not obvious. And by comparing the "Han" curves of all the samples, it can be found that the phase separation phenomenon of the asphalt binder samples is not obvious when the temperature exceeds 70 °C, which also proves the excellent compatibility between SBS/TB crumb rubber and the base asphalt binder.

In addition, the slopes of the logG' versus logG'' curves in the terminal region were determined by linear fitting for the "Han" curves of each asphalt binder sample in this study, as shown in Table 10, it can be seen from the data in the table that the R_2 of SBS/TB crumb rubber modified asphalt binder exceeds 0.97, indicating that the linear fitting model is suitable for fitting the terminal region of logG' versus logG''

Table 9
30 °C Results of modified asphalt binder displacement factor and master curve model fitting parameters at reference temperature.

Displacement factors and the model-fitting parameters	Asphalt binder samples					
	S_2	S_3	S_2R_{10}	S_2R_{15}	S_3R_{10}	S_3R_{15}
$\alpha_{(40\ °C)}$	−0.865	−0.905	−0.988	−0.939	−0.962	−0.996
$\alpha_{(50\ °C)}$	−1.613	−1.687	−1.803	−1.713	−1.754	−1.817
$\alpha_{(60\ °C)}$	−2.266	−2.370	−2.487	−2.362	−2.419	−2.506
$\alpha_{(70\ °C)}$	−2.842	−2.972	−3.069	−2.915	−2.984	−3.092
$\alpha_{(80\ °C)}$	−3.353	−3.506	−3.570	−3.391	−3.470	−3.596
$\log\lvert G^*\rvert_{max}$	5.1759	5.1390	4.8453	5.4840	5.4532	5.7451
$\log\lvert G^*\rvert_{min}$	−5.0731	−4.8379	−6.4360	−6.9190	−6.6960	−6.1837
β	−0.9367	−0.9787	−1.2893	−1.0902	−1.0778	−0.9634
γ	−0.3325	−0.3180	−0.2959	−0.2459	−0.2375	−0.2220
C_1	11.9368	12.4771	10.3031	9.7785	9.9788	10.3487
C_2	127.9991	127.9236	94.2840	94.1817	93.7695	93.8825

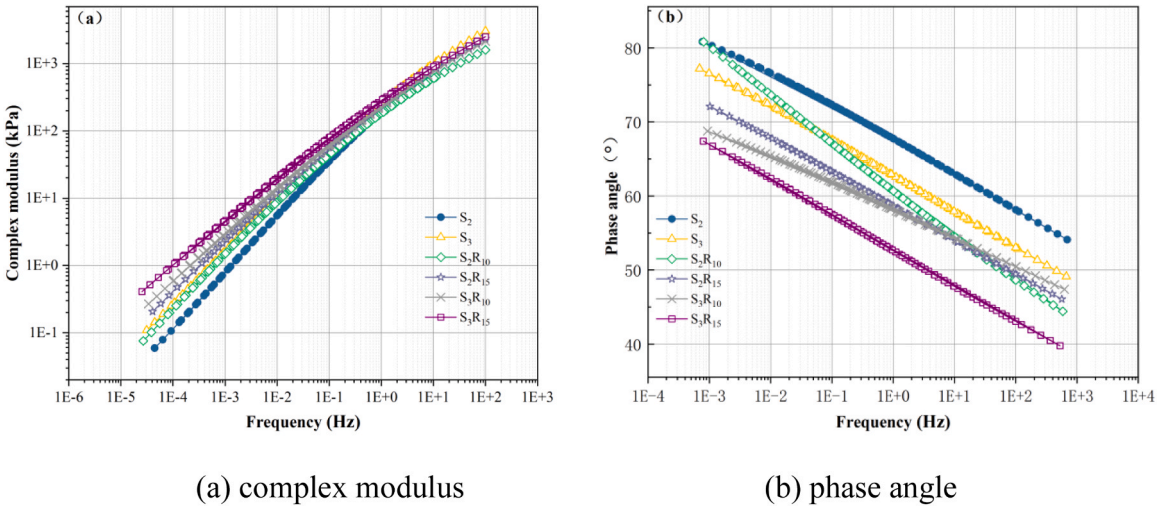

Fig. 13. Modified asphalt binder 30 °C master curve.

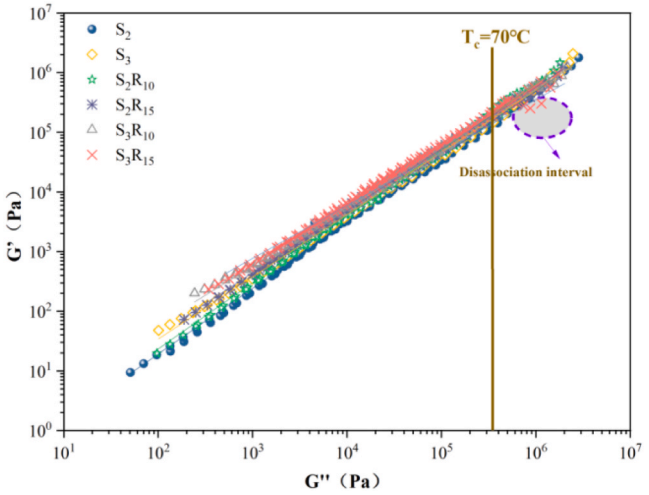

Fig. 14. The Han curve of the modified asphalt binder sample.

curves of the asphalt binder samples. The slope of the curve for S_2R_{10} is closer to 2, which indicates that the sample is more inclined to the homopolymer sample compared to the other binders.

Comparison of the slope of the end region of the Han curve, it can be found that 10 % of TB crumb rubber can improve the compatibility of the modified asphalt binder, but the dosage of 15 %, SBS/TB crumb rubber modified asphalt binder compatibility decreased, which may be due to the low dosage of TB crumb rubber, the depolymerization process of the rubber powder to promote the composite modifier solubility and solubility, but too much TB crumb rubber will exacerbate the agglomeration of the composite modifier and entanglement, resulting in the modified asphalt system of the non-homogeneous nature of the modified asphalt system.

Table 10
Slope of the Han curve.

Asphalt binder samples	S_2	S_3	S_2R_{10}	S_2R_{15}	S_3R_{10}	S_3R_{15}
Gradient	1.10227	1.04347	1.11053	1.03715	0.98547	0.97655
R^2	0.99796	0.99832	0.99822	0.99877	0.99847	0.99627

3.6. *High temperature performance analysis*

3.6.1. *Analysis of PG classification test*

The results of the test of failure temperature of each asphalt binder sample are shown in Fig. 15, and the test results show that the failure temperature of all modified asphalt binders is higher than 64°C. According to the PG classification rules, all modified asphalt binder samples in Fig. 15 can be divided into four grades. Among them, it can be intuitively seen that the difference of failure temperature is significantly related to the SBS content and the amount of TB crumb rubber. Specifically, the improvement of the amount of the two modifying agents is conducive to the improvement of the high temperature grade of the

binder.

In addition, it is easy to find that the failure temperature of S_3 and S_2R_{10} is the same as PG76, and there is no obvious difference, which indicates that on the basis of S_2, SBS content increased by 1 % and 10 % TB crumb rubber is equivalent to the high temperature performance of SBS modified asphalt binder. Among all binders, S_3R_{15} exhibits the highest failure temperature. This is attributed to the addition of higher content SBS and TB rubber powder effectively hinders the flow of asphalt binder under high temperature conditions. And the ability of the asphalt binder matrix to resist permanent deformation is greatly improved, so the rutting factor is less affected by the temperature change.

3.6.2. Analysis of zero shear viscosity test

To ensure the appearance of a viscosity plateau region in the low-frequency domain, the Carreau-Yasuda model [30,31] describing the stress-strain relationship of a pseudoplastic non-Newtonian fluid was chosen to fit the ZSV as shown in Eq. (12).

$$\eta = \frac{\eta_0 - \eta_\infty}{\left[1 + (K\omega)^2\right]^{m/2}} + \eta_\infty \tag{12}$$

Where η_∞ is the shear viscosity limit value and K and m are material parameters.

The results of fitting the relevant parameters of the Carreau-Yasuda model and the complex viscosity-shear rate relationship curves for the six modified asphalt binder samples at 60°C are shown in Table 11 and Fig. 16, respectively. For all samples, the complex viscosity values increase with decreasing shear frequency and show very small variations in the low frequency range, which indicates that at this point the fluid state of the asphalt binder enters the first Newtonian region. It can also be noted that the incorporation of SBS and TB crumb rubber significantly leads to an increase in the rate of viscosity change, which may be related to the structure of the polymer network formed by the high degree of cross-linking of the two polymers. Fig. 17 shows the results of the calculated zero shear viscosity values at 60 °C for the six modified asphalt binder samples, which indicate that the increase in the amount of SBS and TB crumb rubber leads to an increase in the zero-shear viscosity, resulting in an increase in rutting resistance, with S_3R_{15} having better rutting resistance.

3.6.3. Analysis of percent recovery R% and creep compliance Jnr

The average rate of return $R_{0.1}$, $R_{3.2}$ test results for each modified asphalt binder specimen at 0.1 kPa and 3.2 kPa stress levels are shown in Fig. 18(a). The parameters $R_{0.1}$ and $R_{3.2}$ can be used as indicators for evaluating the delayed elastic behavior of the binder, the magnitude of which characterizes the creep recovery capacity of the sample. From Fig. 18(a), it can be seen that S_2 exhibits the smallest $R_{0.1}$ and $R_{3.2}$ among all the asphalt binder samples, which indicates that the 2 % doped SBS modified asphalt binder has the smallest percentage of elastic component under the creep and recovery loading action cycles, reflecting a poor creep recovery capability.

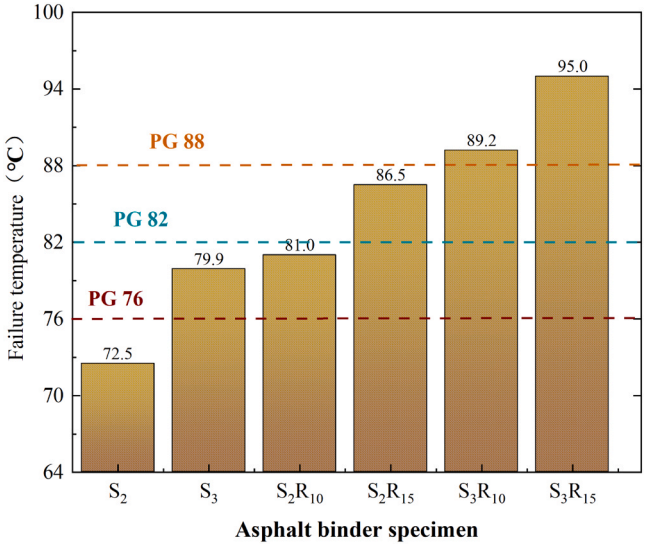

Fig. 15. Failure temperature of each modified asphalt binder test sample.

Compared with S_2, both S_3 and SBS/TB crumb rubber modified asphalt binder showed a significant increase in creep recovery, which indicates that both TB crumb rubber and SBS can provide elastic components for asphalt binder. And the increase in temperature obviously led to the attenuation of the creep capacity of the modified asphalt binder samples, and the amount of creep recovery attenuation of different specimens showed a certain degree of variability, and it was easy to find that all the specimens from 70 °C to 76 °C creep capacity attenuation is greater than that from 64 °C to 70 °C, and the amount of change in the decay of the creep recovery rate of S_3R_{15} is smaller at higher stress levels and temperatures, indicating that it has a more excellent elasticity and resistance to deformation resistance.

Fig. 18(b) shows the results of the non-returnable creep flexibility test for each modified asphalt binder specimen. J_{nr} can be used to characterize the viscosity of asphalt binder, and the smaller the J_{nr} value, the more pronounced high-temperature elasticity the asphalt binder mainly exhibits. From the Fig. 18(b), it can be seen that the relationship between the non-recovery creep softness of each modified asphalt binder specimens are exactly opposite to the creep recovery rate. The Jnr values of each SBS/TB crumb rubber modified asphalt binder specimen were less than S_2 at 0.1 kPa and 3.2 kPa stress levels, indicating that the presence of SBS/TB crumb rubber powder modifier was able to inhibit the generation of asphalt binder irreversible deformation under repetitive loading conditions at 64°C, 70°C and 76°C. And compared to SBS modified asphalt binder, SBS/TB crumb rubber modified asphalt binder exhibits superior rutting performance.

In order to further characterize the sensitivity of each modified asphalt binder sample to the magnitude of the load, stress sensitivity calculations were carried out for the non-recovery creep flexure and creep recovery rate of different modified asphalt binders, and the results of the calculations are shown in Fig. 19. Compared with S_2 and S_3, S_2R_{10}, S_2R_{15}, and S_3R_{10}, S_3R_{15} exhibited lower stress sensitivity, indicating that the addition of TB crumb rubber can effectively compensate for the deficiency of SBS modified asphalt binder in terms of stress sensitivity. Comparison of each composite modified asphalt binder can be visualized that the R_{diff} and $J_{nr\text{-}diff}$ of each asphalt binder specimen exhibit a certain negative correlation with the dosage of the compounding agent. In addition, it is easy to find that SBS/TB crumb rubber modified asphalt binder has more prominent low stress sensitivity at higher temperature conditions, especially S_3R_{15}.

3.7. Low temperature performance analysis

The BBR test results for each modified asphalt binder are shown in Fig. 20. From the results in the figures, it can be seen that the differences in temperature and modifier type have different effects on the S and m values of asphalt binder. For creep strength, the S values of all asphalt binder specimens at −12 °C, −18 °C, and −24 °C temperatures satisfy the recommended requirements of SHRP (less than 300 MPa), indicating good low-temperature performance of the modified asphalt binder. The results of the m-value test show that the m-value of each asphalt binder sample can meet the requirements of use (more than 0.3) only under the condition of −12 °C, when the temperature reaches −18 °C, the m-value of S_2 is slightly lower than the standard value, and when the temperature is as low as −24 °C, only S_3R_{10} and S_3R_{15} can meet the requirements, which proves that the lowering of the temperature is more significant in the deformation capacity of the modified asphalt binder.

Comparing the results of the two figures, it can be seen that at the

Table 11
ZSV fitting results.

The Carreau-Yasuda model fitting parameters	Asphalt binder samples					
	S_2	S_3	S_2R_{10}	S_2R_{15}	S_3R_{10}	S_3R_{15}
η_0	1220.200	4975.412	2538.227	5210.511	11,240.281	18,546.821
K	392.380	274.393	319.794	419.321	494.080	385.076
m	143.591	99.953	116.366	150.635	143.408	139.255
η_∞	124.564	168.961	145.543	180.978	190.443	198.844

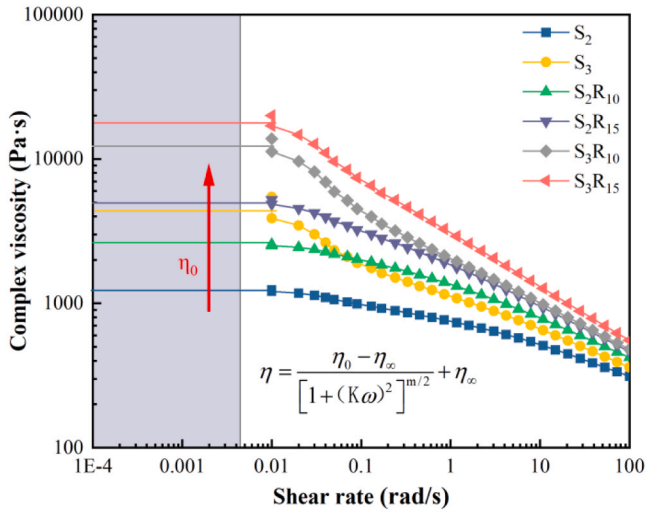

Fig. 16. Viscosity-shear rate curves of the modified asphalt binder samples.

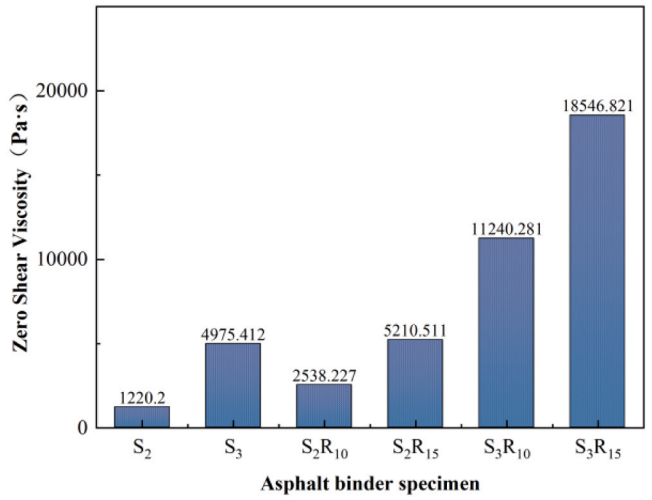

Fig. 17. The zero-shear viscosity of modified asphalt binder based on Carreau-Yasuda model.

same test temperature, the differences in the low-temperature resistance of each modified asphalt binder have consistency, the increase in the dosage of SBS and TB crumb rubber can improve the low-temperature cracking resistance. The improvement of SBS on the S and m values are more obvious, and the improvement of the TB crumb rubber on the two has a differentiated effect, when the temperature is gradually lowered, the increase in the amount of TB crumb rubber dosage makes the S value of the attenuation of the greater amount of increase in the value of the m value of a smaller amount.

3.8. Correlation analysis of microstructural, thermodynamic and rheological parameters

By analyzing the microstructural, thermal stability and rheological properties of SBS/TB crumb rubber modified asphalt binder, we can find that the microstructural, thermodynamic and rheological parameters have the same variation characteristics between them. It is well worth analyzing whether there is a correlation between these three different parameters. Since the microstructural parameter asphalt binder polymer particle area ratio (Area) does not satisfy the normal distribution, it is analyzed in this study by using the Spearman correlation coefficient [32], the formula is shown in Eq. (13), the range of interval of Spearman correlation coefficient is shown in Table 12.

$$r = \frac{\sum_{i=1}^{N}(Ri-\overline{R})(Si-\overline{S})}{[\sum_{i=1}^{N}(Ri-R)^2\sum_{i=1}^{N}(Si-\overline{S})^2]^{\frac{1}{2}}} \tag{13}$$

Where R_i and S_i are the level of values taken for observation i, respectively, $\overline{R}$ and $\overline{S}$ are the average level of variables x and y, respectively, N is the total number of observations.

Because the rheological parameters of SBS/TB crumb rubber modified asphalt binder have more forms, but they are completely replaceable with each other. In order to prevent too many parameters from making it difficult to express the results intuitively, zero shear viscosity (ZSV) and creep strength S at −12 °C (-12 °C S) were chosen as the rheological parameters for the correlation analysis. The Spearman correlation coefficient heat map of the microscopic, thermodynamic and rheological parameters of SBS/TB crumb rubber modified asphalt binder are shown in Fig. 21. The values in Fig. 21 represent the magnitude of the correlation coefficient between two parameters.

As can be seen from Fig. 21, the correlation of Area with T_S and Ea is greater than 0.8, while the correlation of Area with ZSV and −12 °C S is also greater than 0.8, which means that the microstructural parameters have extremely strong correlation with thermodynamic parameters and rheological parameters. In other word, we can greatly control the thermodynamic and rheological properties of SBS/TB crumb rubber modified asphalt binder by controlling the percentage of polymer in asphalt binder.

The correlation coefficient between T_S and Ea is 0.829, which means that the thermodynamic parameters have extremely strong correlation with each other, the correlation coefficient between −12 °C S and ZSV is −1, which is consistent with the conclusion that the rheological parameters can be fully replaced. The correlation coefficients between the thermodynamic parameters and rheological parameters are between 0.8 and 1, which is also an extremely strong correlation, and these two parameters with different property can be predicted with each other to a certain extent, which provides a reference for the subsequent design of asphalt performance.

4. Conclusion

In this study, the micro-modification mechanism of SBS/TB crumb rubber modified asphalt binder was analyzed by FM and FTIR. The storage stability of the modified asphalt binder was analyzed by

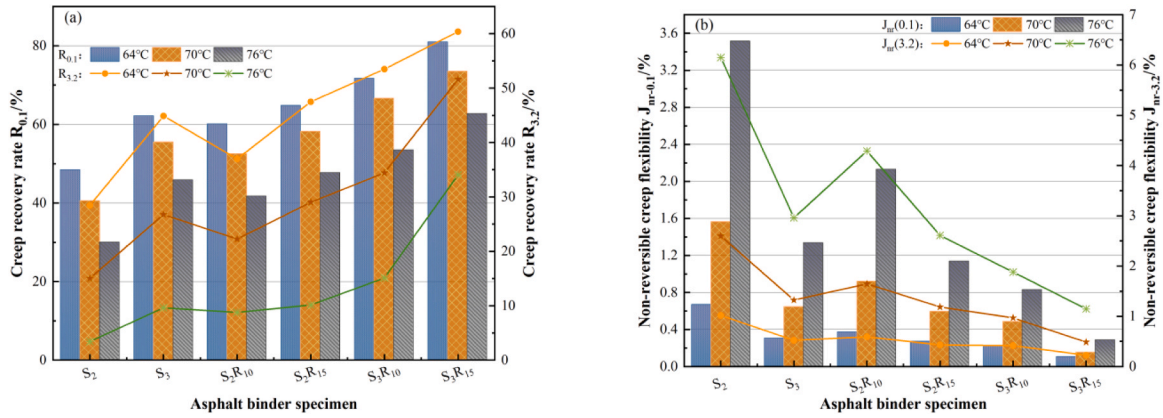

Fig. 18. Results of R and J_{nr}: (a) Mean creep response rate at 0.1 kPa and 3.2 kPa stress levels (b) Mean unrecoverable creep flexibility results at 0.1 kPa and 3.2 kPa stress levels.

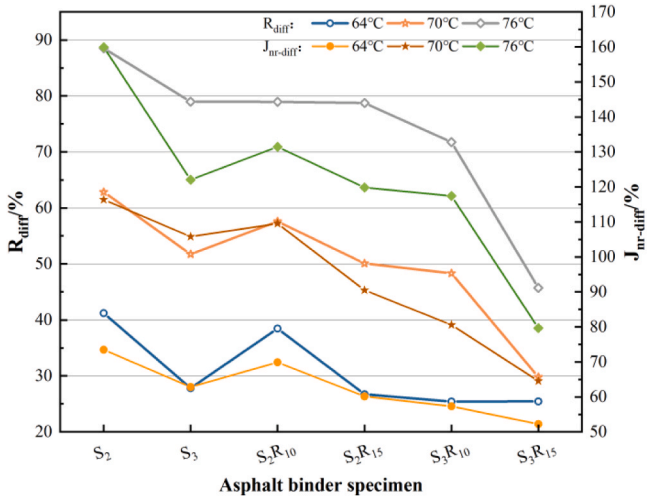

Fig. 19. Stress sensitivity results at 0.1 kPa and 3.2 kPa stress levels.

segregation test. The thermal stability and the reaction mechanism of the modified asphalt binder were investigated by TGA. The rheological properties, high-and-low temperature performance of the modified asphalt binder were comprehensively evaluated by DSR and BBR. Finally, Correlation between microstructural, thermodynamic and rheological parameters analyzed by Spearman correlation coefficient. The main conclusions are as follows:

(1) SBS and TB crumb rubber are uniformly distributed as dispersed phases in asphalt binder, and the two have good compatibility, and the two modifiers can promote each other's reaction, resulting in better modification effects, and SBS/TB crumb rubber modified asphalt binder has better storage stability compared with SBS modified asphalt. In addition, SBS and TB crumb rubber modification processes mainly involve chemical reactions between conjugated double bonds on the benzene ring, $-CH_3$, $-CH_2-$, -C═C-, and C-H on the benzene ring.

(2) Thermal stability of SBS/TB crumb rubber modified asphalt binder increases and then decreases with the increase of SBS and TB crumb rubber dosage. It will have optimal thermal stability when doping is S_3R_{15}, and its Ea can be increased with 61.8 %.

Table 12
|r| value and correlation degree.

|r|	Correlation degree
(0, 0.2]	Extremely weak correlation
(0.2, 0.4]	Weak correlation
(0.4, 0.6]	Moderately correlation
(0.6, 0.8]	Strong correlation
(0.8, 1]	Extremely strong correlation

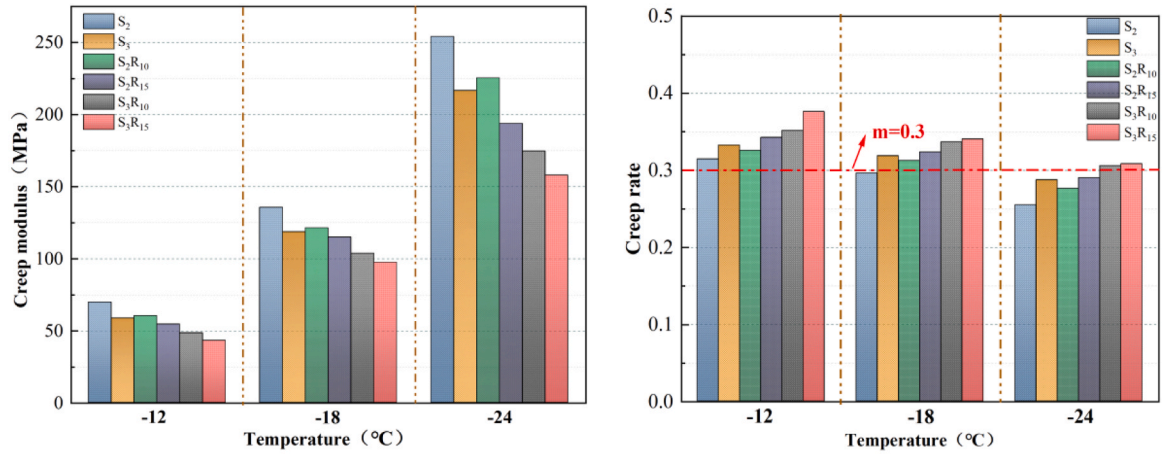

Fig. 20. Test results of the S and m value of the modified asphalt binder.

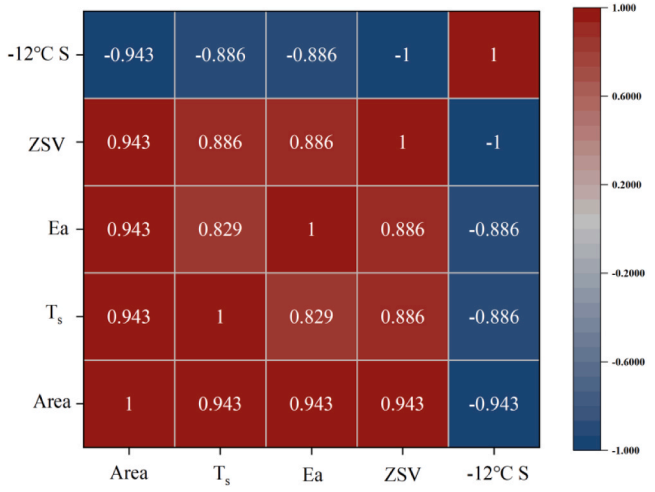

Fig. 21. Heat map of Spearman correlation coefficient.

And based on the kinetic parameters analysis of Flynn-Ozawa-Wall (FOW), Kissinger-Akahira-Sonuse (KAS), SBS/TB crumb rubber modified asphalt binder pyrolysis is One-dimension diffusion or One-dimension phase boundary.

(3) From the master curve, the complex modulus of the samples is quite different, but in the low frequency domain, the complex modulus of all asphalt binders tends to be the same value, and the phase angle shows an approximate linear decrease with the increase of the reduction frequency. And it can be seen that S_2R_{10} is more inclined to the homopolymer sample compared to the other binders from the Han curve.

(4) The failure temperature of S_3R_{15} is the highest, and the ZSV increases with SBS and TB crumb content doping, up to 15 times higher, and resulting in improved rutting resistance of the asphalt binder. SBS/TB crumb rubber modified asphalt binder has more prominent low stress sensitivity at higher temperature conditions, and stress sensitivity can be reduced by more than 50 %.

(5) The synergistic modification of SBS and TB crumb rubber could improve the crack resistance of low temperature, in which SBS improved S and m values, the improvement effect of TB crumb rubber on the two is different. When the temperature gradually decreases, the increase of TB crumb rubber makes the decay of S value larger and the increase of m value smaller.

(6) The microstructural, thermodynamic, and rheological parameters exhibit an extremely strong correlation, and these three parameters with different property can be predicted with each other to a certain extent.

CRediT authorship contribution statement

Shan Huang: Writing – original draft, Data curation. **Huikun Chen:** Data curation. **Dongyu Niu:** Writing – review & editing, Supervision, Methodology. **Shisong Ren:** Writing – review & editing. **Xueyan Liu:** Methodology, Investigation.

Declaration of Competing Interest

The authors declare that they have no known competing financial interests or personal relationships that could have appeared to influence the work reported in this paper.

Acknowledgements

The research is supported by the Natural Science Basic Research Program of Shaanxi (2024JC-YBMS-374), the Fundamental Research Funds for the Central Universities, CHD (300102314902), Shaanxi Housing and Urban-Rural Development Science and Technology Project (2023-K12), Zhengcheng R&D Center (ZCYF-2023-01-01), the Key Research and Development Projects of Qinghai Province (2025-QY-229).

Data availability

Data will be made available on request.

References

[1] H. Chen, S. Huang, D. Niu, Y. Gao, Z. Zhang, Fatigue characterization and assessment methods for the terminal blend crumb rubber/SBS composite modified asphalt binders, Constr. Build. Mater. 430 (2024), https://doi.org/10.1016/j.conbuildmat.2024.137234.

[2] H. Li, C. Cui, A.A. Temitope, Z. Feng, G. Zhao, P. Guo, Effect of SBS and crumb rubber on asphalt modification: a review of the properties and practical application, J. Traffic Transp. Eng. (Engl. Ed.) 9 (5) (2022) 836–863, https://doi.org/10.1016/j.jtte.2022.03.002.

[3] Maciej Sienkiewicz, Helena Janik, Kaja Borzędowska-Labuda, Justyna Kucińska-Lipka, Environmentally friendly polymer-rubber composites obtained from waste tyres: a review, J. Clean. Prod. 147 (2017) 560–571, https://doi.org/10.1016/j.jclepro.2017.01.121.

[4] A. Zhu, Study on the Technology of Preparing Fine Rubber Powder from Waste Rubber Tires, Master thesis, Shanghai Polytechnic University, 2022, 10.27916/d.cnki.ghdeg.2022.000078.

[5] H. Li, Y. Zhang, M. Zhang, C. Cui, G. Hao, L. Zhou, Optimizing parameters for the preparation of low viscosity rubber asphalt incorporating waste engine oil using response surface methodology, Environ. Sci. Pollut. Res. Int. 30 (37) (2023) 87433–87448, https://doi.org/10.1007/s11356-023-28383-2.

[6] M. Liang, X. Xin, W. Fan, H. Luo, X. Wang, B. Xing, Investigation of the rheological properties and storage stability of CR/SBS modified asphalt, Constr. Build. Mater. 74 (2015) 235–240, https://doi.org/10.1016/j.conbuildmat.2014.10.022.

[7] Q. Fu, G. Xu, X. Chen, J. Zhou, F. Sun, Rheological properties of SBS/CR-C composite modified asphalt binders in different aging conditions, Constr. Build. Mater. 215 (2019) 1–8, https://doi.org/10.1016/j.conbuildmat.2019.04.076.

[8] J. Zhou, X. Chen, G. Xu, Q. Fu, Evaluation of low temperature performance for SBS/CR compound modified asphalt binders based on fractional viscoelastic model, Constr. Build. Mater. 214 (2019) 326–336, https://doi.org/10.1016/j.conbuildmat.2019.04.064.

[9] H. Wang, Y. Huang, K. Jin, Z. Zhou, Properties and mechanism of SBS/crumb rubber composite high viscosity modified asphalt, J. Clean. Prod. 378 (2022), https://doi.org/10.1016/j.jclepro.2022.134534.

[10] K. Duan, C. Wang, J. Liu, L. Song, Q. Chen, Y. Chen, Research progress and performance evaluation of crumb-rubber-modified asphalts and their mixtures, Constr. Build. Mater. 361 (2022), https://doi.org/10.1016/j.conbuildmat.2022.129687.

[11] W. Zheng, H. Wang, Y. Chen, J. Ji, Z. You, Y. Zhang, A review on compatibility between crumb rubber and asphalt binder, Constr. Build. Mater. 297 (2021), https://doi.org/10.1016/j.conbuildmat.2021.123820.

[12] Z. Liu, Z. Wang, Development of terminal blend rubber and SBS modified asphalt: a case study, Constr. Build. Mater. 334 (2022), https://doi.org/10.1016/j.conbuildmat.2022.127459.

[13] C. Qian, W. Fan, Evaluation and characterization of properties of crumb rubber/SBS modified asphalt, Mater. Chem. Phys. 253 (2020), https://doi.org/10.1016/j.matchemphys.2020.123319.

[14] S. Wang, W. Huang, Investigation of aging behavior of terminal blend rubberized asphalt with SBS polymer, Constr. Build. Mater. 267 (2021), https://doi.org/10.1016/j.conbuildmat.2020.120870.

[15] J. Zhang, W. Huang, Y. Zhang, C. Yan, Q. Lv, W. Guan, Evaluation of the terminal blend crumb rubber/SBS composite modified asphalt, Constr. Build. Mater. 278 (2021), https://doi.org/10.1016/j.conbuildmat.2021.122377.

[16] W. Huang, M. Zheng, Fatigue performance of terminal blend rubberized asphalt mixture, J. Tong Ji Univ. (Nat. Sci.) 42 (10) (2014) 1543–1549, https://doi.org/10.11908/j.issn.0253-374x.2014.10.013.

[17] T. Xu, X. Huang, Study on combustion mechanism of asphalt binder by using TG–FTIR technique, Fuel 89 (9) (2010) 2185–2190, https://doi.org/10.1016/j.fuel.2010.01.012.

[18] J. Yu, P. Cong, S. Wu, Investigation of the properties of asphalt and its mixtures containing flame retardant modifier, Constr. Build. Mater. 23 (6) (2009) 2277–2282, https://doi.org/10.1016/j.conbuildmat.2008.11.013.

[19] H. Wu, A. Shen, H. Pan, X. Hou, P. Yu, Y. Li, Mechanism of multilayer graphene nanoplatelets and its effects on the rheological properties and thermal stability of styrene–butadiene–styrene modified asphalt, Diam. Relat. Mater. 130 (2022), https://doi.org/10.1016/j.diamond.2022.109434.

[20] S. Cui, N. Guo, Y. Tan, Z. You, Z. Chu, X. Jin, Z. Guo, Preparation and microstructural and thermal properties of a vulcanized Eucommia ulmoides gum modified asphalt, Constr. Build. Mater. 408 (2023), https://doi.org/10.1016/j.conbuildmat.2023.133727.

[21] Y. Li, C. Wang, Z. Wang, B. Zheng, H. Ma, Y. Zhang, Pyrolysis characteristics analysis of cold mix asphalt mixture based on TG-FTIR-GC/MS, J. Anal. Appl. Pyrolysis 177 (2024), https://doi.org/10.1016/j.jaap.2024.106385.
[22] L. Xu, Z. Zhao, J. Li, X. Li, C. Jiang, F. Xiao, Thermal anti-cracking investigation of asphalt-based seal technology for airport base layer in frozen ground region, Cold Reg. Sci. Technol. 204 (2022), https://doi.org/10.1016/j.coldregions.2022.103673.
[23] J. Hao, Y. Che, Y. Tian, D. Li, J. Zhang, Y. Qiao, Thermal cracking characteristics and kinetics of oil sand bitumen and Its SARA fractions by TG–FTIR, Energy Fuels 31 (2) (2017) 1295–1309, https://doi.org/10.1021/acs.energyfuels.6b02598.
[24] L. Tan, S. Wang, T. Xu, W. Xia, Inhibitory effects of composite fire retardant loaded in porous warm-mix agent on asphalt pyrolysis and volatile emission, J. Mater. Civ. Eng. 34 (10) (2022), https://doi.org/10.1061/(ASCE)MT.1943-5533.0004402.
[25] S. Ren, X. Liu, P. Lin, S. Erkens, Influence of swelling-degradation degree on rheological properties, thermal pyrolysis kinetics, and emission components of waste crumb rubber modified bitumen, Constr. Build. Mater. 337 (2022), https://doi.org/10.1016/j.conbuildmat.2022.127555.
[26] AASHTO T313-12. Standard Method of Test for Determining the Flexural Creep Stiffness of Asphalt Binder Using the Bending Beam Rheometer (BBR).
[27] F. Xu, B. Wang, D. Yang, J. Hao, Y. Qiao, Y. Tian, Thermal degradation of typical plastics under high heating rate conditions by TG-FTIR: pyrolysis behaviors and kinetic analysis, Energy Convers. Manag. 171 (2018) 1106–1115, https://doi.org/10.1016/j.enconman.2018.06.047.
[28] Y. Bi, R. Wei, R. Li, J. Zhang, J. Pei, Evaluation of rheological master curves of asphalt mastics and asphalt-filler interaction indices, Constr. Build. Mater. 265 (2020), https://doi.org/10.1016/j.conbuildmat.2020.120046.
[29] M. Zheng, Y. Liu, X. Liu, W. Zhang, F. Wang, S. Liu, Study on the viscoelastic behaviour of the modified asphalt containing multi-walled carbon nanotubes (MWCNTs) and crumb rubber (CR), Constr. Build. Mater. 311 (2021), https://doi.org/10.1016/j.conbuildmat.2021.125244.
[30] D.A. Anderson, Y.M. Le Hir, J.-P. Planche, D. Martin, A. Shenoy, Zero shear viscosity of asphalt binders, Transp. Res. Rec. 1810 (1) (2002) 54–62, https://doi.org/10.3141/1810-07.
[31] S. Biro, T. Gandhi, S. Amirkhanian, Determination of zero shear viscosity of warm asphalt binders, Constr. Build. Mater. 23 (5) (2009) 2080–2086, https://doi.org/10.1016/j.conbuildmat.2008.08.015.
[32] Z. Li, X. Gao, D. Lu, Correlation analysis and statistical assessment of early hydration characteristics and compressive strength for multi-composite cement paste, Constr. Build. Mater. 310 (2021), https://doi.org/10.1016/j.conbuildmat.2021.125260.